# Genetically encoded cell-death indicators (GEDI) to detect an early irreversible commitment to neurodegeneration

Jeremy W. Linsley[1], Kevan Shah[1], Nicholas Castello[1], Michelle Chan[1], Dominic Haddad[2], Jay Mancini[1], Viral Oza[1], David Kokel[3,4], Steven Finkbeiner[1,4,5*]

[1]Gladstone Center for Systems and Therapeutics, San Francisco, CA 94158, USA
[2]Gladstone Institute of Neurologic Disease, San Francisco, CA 94158, USA
[3]Department of Physiology, University of California, San Francisco, CA 94158, USA
[4]Institute for Neurodegenerative Disease, University of California, San Francisco, CA 94158, USA
[5]Neuroscience Graduate Program, University of California, San Francisco, CA 94158, USA; Biomedical Sciences and Neuroscience Graduate Program, University of California, San Francisco, CA 94143, USA; Taube/Koret Center for Neurodegenerative Disease, Gladstone Institutes, San Francisco, CA 94158, USA; Department of Neurology, University of California, San Francisco, CA 94158, USA.

*Corresponding Author: sfinkbeiner@gladstone.ucsf.edu
Gladstone Institutes
1650 Owens St
San Francisco, CA 94138

**Abstract**

Cell death is a critical process that occurs normally in health and disease. However, its study is limited due to available technologies that only detect very late stages in the process or specific death mechanisms. Here, we report the development of a new fluorescent biosensor called genetically encoded death indicator (GEDI). GEDI specifically detects an intracellular $Ca^{2+}$ level that cells achieve early in the cell death process and marks a stage at which cells are irreversibly committed to die. The time-resolved nature of GEDI delineates a binary demarcation of cell life and death in real time, reformulating the definition of cell death. We demonstrate that GEDI acutely and accurately reports death of rodent and human neurons *in vitro*, and show GEDI enables a novel automated imaging platform for single cell detection of neuronal death *in vivo* in zebrafish larvae. With a quantitative pseudo-ratiometric signal, GEDI facilitates high-throughput analysis of cell death in time lapse imaging analysis, providing the necessary resolution and scale to identify early factors leading to cell death in studies of neurodegeneration.

## Introduction

Neurodegenerative diseases such as Parkinson's disease (PD)[1,2], Huntington's disease (HD)[3-7], frontotemporal dementia (FTD), Alzheimer's disease (AD), and amyotrophic lateral sclerosis (ALS)[8,9] are characterized by progressive neuronal dysfunction and death, leading to deterioration of cognitive, behavioral or motor functions. In some cases, neuronal death itself is a better correlate of clinical symptoms than other pathological hallmarks of disease such as Lewy bodies in PD[10], or β-Amyloid in AD[11], and can be used to effectively characterize the relationship of an associated disease phenotype with degenerative pathology[12,13]. Using neuronal death as a consistent and unequivocal endpoint, longitudinal single cell analysis can be performed on model systems to reveal the antecedents and forestallments of cell death[14,15]. Together with statistical tools used in clinical trials that account for variability, stochasticity and asynchronicity amongst individuals within a cohort, it is possible to regress premortem phenotypic markers of neurodegeneration[16], determine which are beneficial, pathological, or incidental to degeneration, and quantify the magnitude of their contribution to fate. For instance, although inclusion body formation is a hallmark of disease in HD and Tar DNA binding protein - 43 (TDP43) ALS, their presence appears to be more consistent with a coping mechanism rather than a causative factor, suggesting clinical intervention to inhibit inclusion body formation could be a misguided approach[3,8]. While there is an ongoing debate about the relative contribution of neuronal dysfunction prior to neuronal death to the clinical deficits that patients exhibit, it is clear that neuronal death marks an irreversible step in neurodegenerative disease. Thus, neuronal death is an important, disease-relevant phenotypic endpoint that is important to understanding neurodegeneration, characterizing the mechanisms of neurodegenerative disease, and developing novel therapeutics.

Nevertheless, precisely determining whether a particular neuron is alive, dead or dying can be challenging, particularly in live imaging studies. Vital dyes, stains and indicators have been developed to selectively label live or dead cells and neurons in culture[17], but the onset of these signals may be delayed until long after a neuron has shown obvious signs of degeneration[12]. Additionally, long-term exposure to exogenous dyes can increase the risk of accumulated exposure toxicity, negating their ability to non-invasively provide information on cell death. Many assays can distinguish between cell death pathways such as apoptosis or necrosis[13] and are conducive to longitudinal imaging[18,19], but these typically require *a priori* knowledge of which cell death pathway is relevant, limiting their utility in neurodegenerative disease, which often involves a spectrum of neuronal death mechanisms[20]. Moreover, cells that begin to die by one cell death pathway may resort to a different one if the original pathway is blocked[21], which can confound analyses. Furthermore, the interpretation and accuracy of apoptotic markers can vary based on the specific cellular system, and some are associated with reversible processes, meaning multiple assays must be used in parallel to unambiguously characterize the precise extent of death within a sample[13,21]. While defining the preferred cell death pathway can give insight into the underlying biology driving cell death, a cell-death pathway agnostic marker is necessary to give an unbiased and reliable readout. In live imaging experiments, the loss of fluorescence of transfected neurons, indicating the rupture of the plasma membrane, has been shown to clearly mark neuronal death[1,3], but fluorescent debris often persists for days after initial morphological signs of death and decay occur, limiting the ability to identify the precise time of death or introducing human error in the scoring of neuronal death by morphology[12]. In summary, without a strict criterion of what constitutes a "point of no return" at

which a neuron's fate is unambiguously sealed, investigation of the causative factors that precede cell death remains challenging.

Although dyes have been used to detect neuronal death *in vivo*[22-24], the permeability of dyes throughout tissue is inconsistent, making quantification difficult. Genetically encoded fluorescent proteins have greatly facilitated the ability to track single neurons within culture[3] and in tissue[25] over time. Furthermore, genetic targeting allows labeling of specific cell subtypes, as well as simultaneous expression of other biosensors, perturbagens, or activators[26]. Some of the most commonly used biosensors in neuroscience are the genetically-encoded $Ca^{2+}$ indicators (GECIs), including the yellow cameleons and GCaMPs/pericams[27,28]. Based on the fusion of circularly permuted fluorescent proteins such as GFP with the $Ca^{2+}$ binding M13-calmodulin domain, GECIs are relatively bright biosensors with low toxicity in neurons[29]. GECIs are used to detect either relative or absolute $Ca^{2+}$ levels or neuronal circuit activity within neurons in culture[30], in tissue[31], within immobilized animals in virtual environments[32,33], and even within freely moving animals[34,35]. The category of GECIs has been diversified and further optimized through the use of alternate fusion proteins to the M13-calmodulin domain as well as targeted mutagenesis[36,37]. Recently, Suzuki et al. engineered endoplasmic reticulum (ER)-targeted calcium-measuring organelle-entrapped protein indicators (CEPIAer) variants that emit either green, red, or blue/green fluorescence to specifically detect $Ca^{2+}$ release events from the ER[37]. In contrast to previously developed ER $Ca^{2+}$ indicator dyes, CEPIAs and newly engineered derivatives[38] can be genetically and subcellularly targeted and are capable of long-term imaging over the lifetime of the neuron, enabling measurement of the full range of calcium dynamics within single neurons over time.

Here, we introduce a new class of GECIs for the detection of cell death in neurons that we call genetically encoded death indicators (GEDIs). We show that GEDIs can robustly indicate the moment when a neuron's ability to maintain $Ca^{2+}$ homeostasis is lost and cannot be restored, providing an earlier and more acute demarcation of the moment of death in a degenerating neuron than previously possible. In combination with a second fluorescent protein fused with a self-cleaving P2a peptide, pseudo-ratiometric GEDIs are easily quantifiable in high-throughput, give highly reproducible signal, and are amenable to long-term imaging. GEDIs can also be targeted to specific neuronal subtypes for imaging *in vivo*. These data establish GEDIs as important new tools for studying the time course of neurodegeneration, providing previously unobtainable delimitation and clarity to the time course of cell death.

## Results

### Development of genetically encoded death indicators

GECIs such as GCaMP6f have been engineered to increase in fluorescence in response to fluctuations in the range of cytosolic $Ca^{2+}$ concentrations that occur during neuronal firing (Figure 1A). The CEPIA GECIs have been engineered with elevated $K_d$ to detect $Ca^{2+}$ transients in organelles such as the ER or mitochondria that contain higher $Ca^{2+}$ (Figure 1A)[37]. We reasoned that removing the ER retention signals and allowing CEPIA variants to localize to the cytosol would render a GECI that was not responsive to activity-based $Ca^{2+}$ transients, but that would increase in fluorescence intensity when cytosolic $Ca^{2+}$ levels approached those of intracellular organelles or the extracellular milieu, which would constitute a catastrophic event for the neuron. We named these reengineered indicators Genetically Encoded Death Indicators (GEDIs). In rat cortical primary neurons, a 10Hz field stimulation caused increased relative fluorescence within cells expressing GCaMP6f but not in those transfected with the red GEDI

variant (RGEDI) (Figure 1B–D). Addition of $NaN_3$, which induces neuronal death, caused increased fluorescence in cells expressing either GCaMP6f or RGEDI (Figure 1B–D). The peak GCaMP6f fluorescence response after stimulation was nearly identical to the fluorescence response to $NaN_3$ treatment; in contrast, the ratio of stimulation to death response in RGEDI expressing cells was close to 0, indicating that the RGEDI sensor preferentially responds to death (Figure 1E). Removal of extracellular $Ca^{2+}$ abrogated the fluorescence response to $NaN_3$ treatment, indicating the primary increase in cytosolic $Ca^{2+}$ was due to influx from the extracellular space, rather than release from intracellular stores (Supplementary Figure 1). To further optimize the RGEDI construct, we appended sequence encoding a porcine teschovirus-1 2a (P2a) "self-cleaving peptide" and EGFP, allowing normalization of the RGEDI signal to EGFP expression (GEDI ratio). This facilitated simple detection of the moment of neuronal death based on a cell's color change when the green and red channels are overlaid (Figure 1F,G).

To assess the ability of RGEDI to detect death in live cell imaging, we used automated longitudinal microscopy[3] to image individual neurons transfected with hSyn1:RGEDI-P2a-EGFP repeatedly at 3 hour intervals (Figure 1H,I). Neurons that died over the course of imaging were marked by clear fragmentation of morphology in the EGFP channel, followed by disappearance of the debris[3,39,40]. Once a cell died, the increase in GEDI ratio remained stable over the course of imaging until disappearance of the debris (Figure 1H,I). In some cases, an increase in GEDI ratio preceded obvious morphology changes (Figure 1H). GEDI signal correlated with and often preceded standard markers for neuronal death such as TUNEL[54], ethidium homodimer D1 (EthD1)[41], propidium iodide (PI)[42], or human curation of the morphology[3] (Supplementary Figure 2). Due to the large separation of GEDI ratio between live and dead neurons, we established a formal threshold of death for the GEDI ratio that could be used to quantify the

amount of cell death in high throughput. Rat primary cortical neurons were transfected with hSyn1:RGEDI-P2a-EGFP in a 96-well plate and the GEDI ratio was derived from each well before and after a subset was exposed to a known cytotoxin, $NaN_3$ (Figure 1J). After 5 minutes, all neurons exposed to $NaN_3$ showed increased GEDI ratio compared to neurons before treatment and those not exposed to $NaN_3$ (Figure 1J). From these data, a GEDI ratio corresponding to the threshold of death (GEDI threshold) was calculated according to equation (1) (See methods).

Automated microscopy was then performed at 24 hour intervals for four days on the remaining 94 wells of the plate, and the previously derived GEDI threshold was used to assess the spontaneous neuronal death of hSyn1:RGEDI-P2a-EGFP-transfected neurons (Figure 1K). In parallel, neuronal death was assessed by manual curation based on the abrupt loss of neuronal fluorescence over time. All neurons identified as live by manual curation had a GEDI ratio below the GEDI threshold, and most neurons identified as dead by manual curation had a GEDI ratio above the GEDI threshold (Figure 1K). The few neurons classified as live by manual curation that contained a GEDI ratio above the threshold were recognized in hindsight to be difficult to classify based on morphology alone. Furthermore, each of these neurons could later be unequivocally classified as dead due to loss or fragmented pattern of fluorescence at the next imaged time point (Supplementary Figure 3A), suggesting an error or inability of humans to correctly classify, and demonstrating GEDI is a more acute and accurate means of classifying neuronal death than manual curation. To examine the possibility that a temporarily increased GEDI ratio signal may give a false positive death indication, a large longitudinal data set of time lapse GEDI images containing 94,106 tracked neurons across multiple imaging conditions was generated (Supplementary Table 1). Across all 32 longitudinal experiments, a consistent GEDI threshold indicating cell death could be established (Supplementary Figure 3B–C). Only 0.28%

of all neurons exhibited a GEDI ratio above the threshold at one time point that subsequently decreased below the death threshold (Supplementary Figure 3D). Upon closer examination of those 304 neurons, each was subsequently found to have an automated segmentation artifact, which distorted the ratio of RGEDI to GFP or a tracking artifact that confused objects, rather than decreased RGEDI signal in relation to GFP (Supplementary Figure 3E). No neurons were found to "die twice," as would be indicated by two fluctuations in GEDI ratio above the death threshold. These data show that the GEDI signal is unlikely to increase above the GEDI threshold in a neuron that is not dead. Therefore, we conclude that GEDI is a biosensor that specifically signals an early and irreversible commitment to degeneration and death and can serve as a ground truth for quantifying cell death.

**Automated identification of toxin resistant and sensitive subpopulations of neurons**

We predicted that by combining GEDI and time lapse imaging, we would be able to monitor a heterogeneous death process and identify time-resolved subpopulations of neurons with differing sensitivities. Glutamate is the most common neurotransmitter in the brain[43], but glutamate excess occurs in neurodegenerative disease and has been shown to be toxic to specific subpopulations of neurons[44]. Glutamate toxicity induces either apoptosis[44] or necrosis[45], and a reliable death sensor capable of detecting either death type can facilitate an unbiased accounting of toxicity. In principle, GEDI should be able to detect all cell death events, as it detects loss of plasma membrane integrity rather than a specific substrate of a cell death pathway. To assess glutamate toxicity, rat primary neurons were transfected with hSyn1:RGEDI-P2a-EGFP and followed with automated microscopy after exposure to different levels of glutamate (Figure 2A, B). A GEDI threshold was used to define dead neurons, and Kaplan-Meyer survival curves were

generated for the time course of imaging (Figure 2C). While over 90% of neurons died within 3 hours of exposure to 0.1mM and 1mM glutamate, recognizable by the stark change in composite GEDI color of images of wells (Figure 2A, B), sparse neurons resistant to those treatments could be identified by their low GEDI ratio that remained alive in the culture long after the initial wave of death. Some neurons remained alive to the end of the 108 hour imaging window in the presence of glutamate (Figure 2C, D).

It is known that GFP and RFP are differentially sensitive to lysosomal proteases, and that differential sensitivity has been exploited to develop tandem tag biosensors to measure autophagy[46]. Since $Ca^{2+}$ is known to activate certain proteases[47], we wondered if differential degradation rates of RGEDI and EGFP fluorescence signals in dead neurons could cause the GEDI ratio to fluctuate and under- or overrepresent death. To investigate, we characterized the decay rate of EGFP and RGEDI signals after rapid death from glutamate toxicity. In dead neurons, the relative fluorescence of each protein decayed at equivalent rates ($t_{1/2}$ = 20.45 hours RGEDI, 20.73 hours EGFP), indicating the activated GEDI ratio is a stable indicator of death across long time intervals of imaging during which neuronal debris remains present (Figure 2E, F). These data suggest that GEDI is a powerful tool to accurately identify live neurons within a culture in which extensive death has occurred.

**Automated survival analysis of multiple neurodegenerative disease models in different species with GEDI**

Neurodegenerative disease-related neuronal death is associated with a spectrum of death mechanisms including apoptosis, necrosis, excitotoxicity, and autophagic cell death[20,48], necessitating the use of a death indicator of all types of cell death for effective and unbiased

detection of total death. To test the effectiveness of GEDI across neurodegenerative disease models, hSyn1:RGEDI-P2a-EGFP was cotransfected into rat cortical primary neurons with pGW1:HttEx1-Q25 or pGW1:HttEx1-Q97, pCAGGs:α-synuclein, or pGW1:TDP43 to generate previously characterized overexpression models of HD[3], PD[40] and ALS or frontotemporal dementia (FTD)[49], respectively (Figure 3A). Each model has been associated with multiple types of cell death to varying degrees[50-53]. In each model, neurons with characteristic yellow overlays of the RGEDI and EGFP channel could be detected at 24 hours (Figure 3A–A''). GEDI ratios for neurons in each model and control at each time point were quantified, and a GEDI threshold was calculated using a subset of neurons designated dead or live by manual curation (Figure 3A–B). GEDI ratios from dead neurons in disease models were lower than GEDI ratios from controls, likely due to the combined effects of reduced total exogenous protein expression observed in each disease model compared to control, and lower separation of GEDI ratio between live and dead neurons at lower RGEDI-P2a-EGFP expression levels (Supplementary Figure 4). High expression of GEDI likely correlates with high expression of co-transfected disease-causing protein, resulting in neurons with high exogenous protein expression levels to die and disappear sooner, causing underrepresentation of high expression of GEDI in disease models (Supplementary Figure 4). Nevertheless, a clear separation of live and dead neurons could still be observed in each case (Figure 3B). Using the labels generated from the GEDI threshold a cumulative risk-of-death (CRD), a statistical measure of survival used in clinical studies[54], was generated showing significant toxicity of each model compared to controls as previously reported (Figure 3C). This showed that GEDI can be used to report toxicity over time across a variety of neurodegenerative disease models.

Cell-based overexpression models of neurodegeneration can be difficult to interpret because protein expression above physiological levels can introduce artifacts, which could also affect GEDI quantification. Neurons derived from induced pluripotent stem cells (iPSC) have the advantage of maintaining the genomic variants of the patients from whom the cells came, facilitating modeling of neurodegenerative diseases[55]. To test whether GEDI can detect death in an iPSC-derived model of neurodegeneration in which the endogenous disease-causing protein is expressed at physiologically relevant levels, motor neurons (MNs) were derived from iPSCs from normal control patients and compared to neurons derived from patients with a D90A SOD1 mutation, which has been shown to cause ALS[56]. iPSC MNs generated from patients fibroblasts that carry the D90A SOD1 mutation have been previously shown to model key pathologies associated with ALS, such as neurofilament containing inclusions and axonal degeneration, though a clear survival phenotype using a CRD to evaluate toxicity over time has not been established[57]. Neurons were transfected with hSyn1:RGEDI-P2a-EGFP after 19 days of differentiation, and imaged every 12 hours with automated microscopy (Figure 3D–F). The GEDI ratio was quantified and a GEDI threshold was derived and used to generate a CRD plot, which showed that SOD1-D90A containing neurons exhibited increased risk of death compared to controls, with an CRD of 1.26 (Figure 3G). These data show that GEDI can be used to automatically detect neuronal death and derive CRDs from human neurons.

**Development of an expanded family of GEDI sensors**

To expand the applications of the GEDI biosensor, we tested other GEDI variants with alternative characteristics useful in different capacities. Reliance on green and red emission spectra for death detection with RGEDI-P2a-EGFP restricts the ability to concurrently image

other biosensors whose spectra overlap, limiting the opportunity to investigate other co-variates of disease[14]. Accordingly, we engineered RGEDI-P2a-3xBFP, so that death can be reported during simultaneous imaging of green biosensors. Though the GEDI ratio derived from RGEDI-P2a-3×BFP has a smaller dynamic range due to the relative dimness of BFP, the rate of signal increase following exposure to $NaN_3$ was not different between RGEDI-P2a-3×BFP and RGEDI-P2a-EGFP or GCaMP6f-P2a-mRuby[58] (GEDI ratio= GCaMP6f/mRuby) (Figure 4A–D ANOVA p=0.44).

Next, we tested a newly engineered ER $Ca^{2+}$ sensor based on the GCaMP GECI called GCaMP6-150, which was recently reported to have an excellent dynamic range[38] and higher affinity for $Ca^{2+}$ than RGEDI (Figure 4E). We generated a new GEDI sensor based on the GCaMP6-150 template by removing the ER signaling peptides from the GCaMP6-150 cassette and combining it with a P2a peptide and mApple to generate GC150-P2a-mApple. As expected, cells expressing GC150-P2a-mApple showed increased GEDI ratio (GEDI ratio=GC150/mApple) after $NaN_3$-induced death (Figure 4D–F).

GECIs targeted to the nucleus have been shown to increase resolution and duration of signal in whole brain studies of zebrafish[59]. Therefore, we generated GEDI constructs with nuclear localization signals (NLS): GC150-NLS-P2a-mApple-NLS and RGEDI-NLS-P2a-EGFP-NLS (Figure 4F,G). Each nuclear localized GEDI showed a similar increase in GEDI ratio upon NaN3 treatment, corresponding to the death of neurons (Figure 4D,G,H). The kinetics of the responses were not different between any of the GEDI variants ($\tau$ range= 4.7–6.4 minutes, ANOVA p=0.75), indicating similar ability to detect death across imaging situations in which different versions of GEDI are needed (Figure 4D). These data demonstrate that the GEDI

approach offers an acute, versatile, and quantitative method to detect neuron death in time lapse imaging.

**GCaMP acutely reports death *in vivo***

Many zebrafish larvae models of neurodegeneration have been developed, in part to take advantage of their unique characteristics, including translucent skin and the ability to be immobilized for long periods of time, that make them amenable to live imaging[60,61]. However, it has not been possible to acutely detect neuronal death and characterize the preceding events *in vivo* with time lapse imaging in these models, limiting the characterization of neuronal death to static snap shots of single time points[62-64].

We sought to develop a platform to visualize neuronal death longitudinally *in vivo* with GEDI by adapting our automated 4-dimensional longitudinal single cell tracking microscopy platform[25] to *in toto* longitudinal imaging of live zebrafish larvae over multiple days (Supplementary Figure 5). Larvae at 72 hours post fertilization were anaesthetized in tricaine, immobilized in low melting point agarose in 96 well optical ZFplates (Diagnocine), where they can typically remain alive for 120 hours as assayed by heartbeat. Automated confocal microscopy was used to repeatedly image each fish in three dimensions at specified intervals, generating 4 dimensional (4D) images of each fish in an array (Supplementary Figure 5). To induce neuronal death, the inducible cell ablation protein nitroreductase (NTR)[65] was expressed in MNs using the *mnx1* promoter[66], and 10 μM of metronidazole (MTZ), a harmless prodrug that is activated by NTR, was added to the zebrafish media. By 24 hours after addition of MTZ, some motor neuron axons became clumped and motor neuron cell bodies looked fragmented compared to DMSO, yet no difference in motor neuron axon area was detected (Figure 5A–C). By 48 hours

after addition of MTZ, motor neuron axons appeared to retract, and a reduction in axon area could be detected, yet somas and/or debris from the MNs remained in the spinal cord (Figure 5A,B). In contrast, non-immobilized mnx:Gal4; UAS:mCherry;UAS:EGFP zebrafish larvae became immotile upon incubation with MTZ for 24 hours, swimming no more than larvae in which the neuromuscular junction has been blocked with botulinum toxin (UAS:BoTx-EGFP)[67] (Figure 5D), indicating that 24 hours incubation in MTZ is sufficient to functionally ablate MNs. Neuronal death at 24 hours post MTZ was also confirmed with the use of PhiPhiLux G1D2a live fluorescent reporter of caspase-3-like activity[23,68] (Supplementary Figure 6A–C). These data suggest that an acute marker for neuronal death is required to monitor neurodegeneration *in vivo* that more accurately distinguishes live neurons from dead neurons.

GCaMP is commonly and widely used in zebrafish for studies of neuronal activity and functionality[69], and transgenic lines with GCaMP expression in the nervous system are widely available, making it easy to apply to studies of neuronal death. GCaMP signal due to endogenous $Ca^{2+}$ transients in MNs is not distinguishable from signal due to loss of membrane integrity associated with neuronal death (see Figure 1). However, we found that GCaMP can be rendered a GEDI within the zebrafish by blocking endogenous neuronal activity with the use of tricaine, an anesthetic that blocks voltage-gated channels in the nervous system[70] even when the motor swimming circuit was activated by application of 0.1% Acetic Acid (AcOH), which stimulates swimming[71] (Supplementary Figure 7A–B). In contrast, with the use of a muscle contraction blocker 4-Methyl-N-(phenylmethyl)benzenesulfonamide (BTS) which immobilizes larvae but does not block neuronal activity[72] GCaMP7 calcium transients are still present (Supplementary Figure 7C–E) . GCaMP7 signal significantly increased from baseline in MNs after 24 hours of MTZ application compared to those incubated in DMSO alone or those not expressing NTR

(Figure 5G–I, Supplementary Figure 8A–B). Similarly, *cacnb1*$^{-/-}$ mutants, which are immobile due to loss of skeletal muscle function but maintain normal MN activity[73], also showed increased GcaMP7 signal in response to MTZ treatment without tricaine immobilization (Supplementary Figure 8A–C). Thus, GCaMP7 can be used as a GEDI and an accurate measure of neuronal death in immobilized zebrafish.

**GEDI150 acutely reports death *in vivo* and is insensitive to $Ca^{2+}$ transients**

Although GCaMP is effective at labeling neuronal death within tricaine-anaesthetized larvae, tricaine application can have adverse effects on physiology[74], The dampening of neuronal activity within the zebrafish can potentially complicate the interpretation of neurodegenerative disease models, especially those in which hyperexcitibility is thought to be a disease-associated phenotype such as AD, FTD and ALS[75,76]. Thus, a true GEDI would be preferable to GCaMP because it would eliminate the need for immobilization in zebrafish imaging preparations in which CNS activity is preserved, such as fictive swimming assays[72,73,77]. We first tested the ability of RGEDI-P2a-EGFP to detect neuronal death *in vivo* by co-injecting DNA encoding *neuroD*:NTR-BFP and *neuroD:*RGEDI-P2a-EGFP at the 1-cell stage, and then using *in toto* live longitudinal imaging to track fluorescence of co-expressing neurons within the larval spinal cord after NTR-MTZ mediated ablation beginning at 72hpf (Figure 6A). After 24 hours of incubation in 10 μM MTZ, the morphology of neurons showed signs of degeneration including neurite retraction and loss of fluorescence, yet neurons co-expressing NTR-BFP and RGEDI-P2a-EGFP did not show increases in GEDI ratio (Figure 6B,C), indicating RGEDI signal cannot distinguish live from dead neurons in this system.

We hypothesized that extracellular $Ca^{2+}$ levels *in vivo* within the zebrafish larvae could be too low to reach the concentration required for RGEDI to optimally fluoresce. Therefore, we next tested if GC150, which has a higher binding affinity for $Ca^{2+}$ (Figure 4E), could better report neuronal death *in vivo*. Sporadic expression of GC150-P2a-mApple was generated by co-injection of DNA encoding *neuroD*: GC150-P2a-mApple with *neuroD*:NTR-BFP at the 1-cell stage. Live longitudinal imaging was performed on larvae incubated in either DMSO or 10 μM MTZ, and individual neurons within the brain expressing both mApple and BFP were tracked in 4D within the whole larvae (Figure 6D–F). Larvae exposed to 10 μM MTZ showed increased GC150 signal by 24 hours after MTZ extending to 48 hours, while larvae exposed to DMSO alone did not show signs of neuronal death or increases in GC150 (Figure 6D–F). With increased binding affinity compared to RGEDI, GC150 could potentially be more susceptible to detecting physiological $Ca^{2+}$ transients within neurons, similar to GCaMP, which could confound its utility as a GEDI. To test whether GC150 increases in fluorescence during $Ca^{2+}$ transients, GC150 was targeted to MNs by injection of *mnx1*:GC150-P2a-mApple. Larvae were immobilized in BTS, and no response of GC150 was detected after activation of the motor circuit, indicating GC150 signal does not increase in response to normal calcium transients within neurons (Supplementary Figure 7F–G). These data indicate GC150 is suitable for *in vivo* detection of neuronal death in an un-anaesthetized animal.

## Discussion

The study of neurodegenerative diseases has been hampered by an inability to distinguish populations of neurons destined to die from those that have already perished, which precludes the investigation of mechanisms that drive selective degeneration. Here, we characterize a novel

biosensor GEDI, which is specifically tuned to detect neuronal death in longitudinal imaging studies, facilitating analysis of neurons in time points leading up to neuronal death. Using automated microscopy, we show that the analysis of GEDI is compatible with fully automated, single cell survival analysis, which has been previously shown to be 100–1000 times more sensitive than population-based studies that rely on a single snapshot in time[26]. We believe this tool will lead to more precision in discovery of the mechanisms of neurodegeneration and increase the throughput of quantitative studies to discover novel therapeutics.

Similar to other death-pathway agnostic indicators of cell death or viability, GEDI detects the loss of membrane integrity as a readout of cell death[78]. However, by uniquely measuring the $Ca^{2+}$ permeability of the membrane, GEDI holds several key advantages for longitudinal imaging. For one, unlike death indicators that rely on DNA intercalation, such as EthD1, PI, or 4′,6-diamidino-2-phenylindole (DAPI)/Höechst, GEDIs are non-toxic. Additionally, intercalating agents require breach of both the plasma membrane and the nuclear membrane, which can be problematic in the stochastic process of degeneration and could result in delayed signal (Supplementary Figure 2). In contrast, each indicator we used to engineer GEDIs binds $Ca^{2+}$ in less than a second[37,38,79], which is over 500× faster than the time course of death after $NaN_3$ exposure (Figure 4). GEDIs can also be combined with complementary labels specific for cell death pathways (Supplementary Figure 2a), which could help resolve ambiguity in cell death pathway crosstalk such as when a cell resorts to a different cell death pathway when the primary pathway is blocked[21], by providing more direct temporal linkage between death pathway signal and death. The stability of the fluorescence tags used in the GEDIs (Figure 2D), enables the signal to be sampled at long time intervals such as every 24 hours, a particularly important property during long-term imaging studies to minimize phototoxicity. These properties allowed

us to use GEDIs to empirically determine the level of cytosolic $Ca^{2+}$ associated with an irreversible fate (Figure 1, Supplementary Figure 3), a property no other death indicator is capable of, to our knowledge. Furthermore, with the increased time resolution of death possible using GEDI, subpopulations of death-resistant neurons and the spread of neuronal death can now be imaged. For instance, reports of subpopulations of neurons displaying resistance to glutamate have been described in culture and *in vivo*[80-83], yet each report has relied on dyes to characterize death at static time points, limiting the ability to resolve the time coarse and cell-to-cell transmission of excitotoxic injury on a single cell level now possible with GEDI (Figure 2A–D). While this study focused on the use of GEDI in degenerating neurons, it should be noted that most if not all cells maintain a concentration gradient of $Ca^{2+}$, suggesting that these death indicators could be adapted for use to report cell death and spread of cell death in other cell or tissue types[84].

Although much of what we know about the etiology of neurodegenerative disease has come from 2-dimensional culture of neurons, it is becoming increasingly clear that the progression of neurodegenerative disease is dependent on the relationship of neurons to their surrounding tissue. For instance, multiple neurodegenerative diseases are linked to abnormal circuitry[75,76,85,86], and evidence suggests that propagation of neurodegenerative disease throughout the brain may proceed via the spread of pathogenic proteins[87-89]. To study such cell non-autonomous phenomena of neurodegeneration, an approach that integrates the 3-dimensionality of tissue is required. Previously, we used organotypic slice culture to create a more tissue-like environment in which to study neurodegeneration over time, with an automated 4D imaging platform[90]. Here, in combination with GEDI, we apply this technology to a zebrafish model of neurodegeneration to study neuronal death *in vivo*. In contrast to organotypic slice

culture models, which expose neurons to stresses of brain dissection and culturing, *in vivo* 4D imaging of zebrafish larvae fully preserves the architecture of the brain. Zebrafish larvae studies can also be scaled up for high-throughput imaging screens[91], and to our knowledge our platform represents the first optimized for 4D longitudinal imaging of immobilized fish. This can be especially useful, as zebrafish larvae are a well characterized behavioral model[92,93], and 4D imaging can be used in parallel with behavioral analysis, providing an important behavioral correlate of neurodegeneration over time.

Our use of 4D imaging of zebrafish generated several important findings. First, we show that the loss of fluorescence is not an acute indicator of neuronal death *in vivo* (Figure 5). One implication of this finding is that studies of neurodegeneration using fluorescent proteins in zebrafish could underestimate the time course of degeneration in the model, and behavioral characterization may be a more acute indicator of degeneration. Time lapse imaging of zebrafish neurodegeneration is also complicated by the species' high neuronal regeneration capacity[94] and the presence of scavenger cells such as microglia[62], which could alter the apparent rate of death over time, underscoring the necessity of an acute indicator to track neurons as they die over time. Second, our successful application of GCaMP7 to detect neuronal death in tricaine-immobilized zebrafish larvae means that commonly used GECIs, under neuronal paralytic conditions, can act as GEDIs. While GECIs prove to be a convenient tool for the study of neurodegeneration, this finding should also raise caution in the interpretation of GECI systems under conditions in which neuronal death occurs, as a chronic increase in GECI signal after death could be confused with normal $Ca^{2+}$ transient activity. Finally, we showed that although RGEDI construct could not be used to detect death *in vivo*, GC150 and GCaMP7 could. Due to the differences in $Ca^{2+}$ binding affinity between the three indicators, these data suggest that free $Ca^{2+}$ in the extracellular spaces

in brain of the zebrafish larvae is somewhat limited and may be insufficient to induce the RGEDI fluorescence upon cell death. Thus, the difference in functionality of RGEDI in cultured neurons (Figures 1–4) and *in vivo* in the zebrafish brain (Figures 5–6), could be due to the virtually unlimited supply of $Ca^{2+}$ in culture medium compared to the brain, where extracellular $Ca^{2+}$ can be limiting in times of high activity[95] and in dense synaptic areas[96]. Interestingly, the limited extracellular $Ca^{2+}$ in our *in vivo* assays raises the intriguing possibility that the sequestration of free calcium in debris of dead neurons could be a previously unexplored mechanism of cognitive decline in neurodegeneration. Future studies using 4D modeling will be key to address this question.

With few disease modifying therapies for neurodegenerative diseases available, there is a great need to understand disease mechanisms and etiology to develop new therapeutic targets[12]. Our studies using neurodegenerative disease models of PD, ALS/FTD, Huntington's disease, glutamate toxicity, and *in vivo* neuronal ablation demonstrate the ability of GEDIs to acutely identify the moment of death in time lapse imaging studies, allowing a unique time-resolved view of neurodegeneration. We believe the use of GEDIs will aid longitudinal single cell analysis of neurons to complete our understanding of the underlying causes of neurodegeneration, and provide assays to help generate much needed therapeutics.

## Methods

### Animals and Culturing

All animal experiments complied with UCSF regulations. Primary mouse and rat cortical neurons were prepared at embryonic days 20–21 as previously described[97]. Neurons were plated in a 96 well plate at $0.1 \times 10^6$ cells per well and cultured in neurobasal growth medium with

100× GlutaMAX, Pen/Strep, and B27 supplement (NB medium). Zebrafish embryos raised to 48hpf were enzymatically dechorionated using 2mg/ml Pronase (Protease, Type XIV, Sigma) for 20 minutes. For behavioral analysis, embryos at 72 and 96 hpf were lightly tapped on the tail with #2 forceps while recording a 10s movie and analyzed as previously described[98]. A list of all zebrafish lines used in this study are available in Supplementary Table 2.

**Plasmids, Transfections, Toxins, Dyes and Injections**

The mammalian expression constructs phSyn1:RGEDI-P2a-EGFP, phSyn1:RGEDI-P2a-3xTagBFP2, phSyn1:RGEDI-NLS-P2a-EGFP-NLS, and phSyn1:TDP43, phSyn1:empty were generated by synthesizing the insert into a pBluescript Sk+ backbone. All constructs were verified by sequencing. At 4–5 d in vitro (DIV), rat cortical neurons were transfected with plasmids and Lipofectamine 2000 to achieve sparse labeling of neurons within each well as previously described[39]. For survival analysis, each well of a 96-well plate containing primary rat cortical neurons was cotransfected with 0.15 µg of DNA of phSyn1:RGEDI-P2a-EGFP, phSyn1:RGEDI-P2a-3xTagBFP2, phSyn1:RGEDI-NLS-P2a-EGFP-NLS, and phSyn1:mRuby-P2a- GCaMP6f[58], 0.1 µg of DNA of phsyn1:empty, pGW1-HttEx1Q97-mCerulean, pGW1-HttEx1Q25-mCerulean[3], or 0.075 µg of DNA pCAGGS–α-synuclein[40] or phSyn1:TDP43. L-Glutamic acid monosodium salt was diluted in NB media with 0.5% DMSO. 2% $NaN_3$ (Sigma) was dissolved in NB media, or in PBS with or without $Ca^{2+}$. For TUNEL staining, the Alexa647 Click-iT Assay for in situ apoptosis detection was used (Life Technologies). For testing other cell death indicators, mouse primary cortical neurons were isolated from embryonic 17 day pups and at 3 DIV, neurons were transfected with either 0.02ug of hSyn1:RGEDI-P2a-EGFP or pGW1-EGFP. At 6 DIV, neurons transfected with RGEDI were treated with neural basal media

while neurons transfected with EGFP were treated with 1uM ethidium homoder-1 Life Technologies) or 0.5uM propidium iodide (Life Technologies). Dyes were allowed to incubate for 30 minutes before a pretreatment timepoint was taken. Neurons were exposed to 90 seconds UV light with a custom-built LED light box to induce cell death and cells were imaged every 4 hours to track the signal of death indicators.

For field stimulation experiment primary mouse neurons were cultured for 4 days before transfection with phSyn1:RGEDI-P2a-EGFP or phSyn1:mRuby-P2a-GCaMP6f , and then imaged at 8 DIV in Tyrode's medium (pH 7.4; in mm: 127 NaCl, 10 HEPES-NaOH, 2.5 KCl, 2 MgCl2, and 2 CaCl2, 30 mm glucose and 10 mm pyruvate) using a Nikon CFI Plan Apo ×40/0.95 air objective on a Nikon Ti-E inverted microscope with an iXon EMCCD camera (Andor Technology). Field stimulation (3s*30Hz) was done after 7s of baseline recording using an A385 current isolator and a SYS-A310 Accu pulser signal generator (World Precision Instruments). 2% $NaN_3$ was added by directly injecting into the imaging chamber after 30s to achieve immediate mixing. GCAMP6f and RGEDI fluorescence images were obtained using the following filters [490/20(ex),535/50 (em) and 543/22 (ex), 617/73 (em) respectively, Chroma] and regions of interest were drawn over cell bodies. The fold change ($\Delta F/F0$) in fluorescence was calculated for each time point after background-subtraction.

To generate zebrafish constructs, gateway recombination-based cloning was performed (Life Technologies) using the Tol2kit[99]. A pME entry clone was generated for RGEDI-P2a3xBFP and RGEDI-P2a-EGFP by subcloning from phSyn1:RGEDI-P2a3xBFP, phSyn1:RGEDI-P2a-EGFP, or phSyn1:GCaMP6f-P2a-mRuby using the pCR8/GW/TOPO TA cloning kit (Life Technologies). pME:GC150-P2a-mApple, and pME-NTR-BFP were synthesized (Genscript) and cloned into pET-30a. Each was combined with p5E-neuroD[100], P3E

polyA and pDestTol2pA[99], to generate *neuroD*: RGEDI-P2a-EGFP, *neuroD*: GC150-P2a-mApple and *neuroD*:NTR-BFP. Embryos were injected at 1-cell stage into the yolk with ~20nl containing 100ng/ul of each DNA. A list of all constructs used in this study are available in Supplementary Table 3.

**In toto automated 4D high content immobilized zebrafish imaging**

For imaging experiments, zebrafish embryos were dechorionated at 24hpf, sorted for fluorescence, and put into 200 μM 1-phenyl 2-thiourea (PTU) E2 medium at 28.5°C to inhibit melanogenesis[101]. At 72hpf embryos were immobilized in 0.05% tricaine methanesulfonate (Sigma) or 50 μM BTS (Tocris) for an hour, then were loaded into wells of a ZFplate (Diagnocine) in 100ul of media with paralytic using wide bore tips and allowed to settle into the slits. Using a multichannel pipette, 100ul of molten 1.5% low melting point agarose was loaded into each nozzle hole, and then 100ul of agarose/paralytic mixture was immediately removed and agarose was allowed to solidify. Finally, liquid media was added to the top of each well containing paralytic with DMSO and/or with 10uM MTZ (Sigma).

The automated spinning disk confocal imaging system was previously described[25]. Briefly, a custom system was used combining a Nikon microscope base (Nikon Ti-E), a Yokogawa spinning disk confocal (Yokogawa CSU-W1), an automated three axis stage (Applied Scientific Instrumentation, MS-2500-Ti and PZ-2300), and modified custom software allowing automated return to the same location on the imaging plate allowing continual imaging of the same location in 3D space. To accommodate zebrafish imaging at 28.5°C rather than at the enclosure temperature of 37°C for mammalian cell culture, a custom-made homeostatic peltier

cooling lid was designed and constructed (Physiotemp) to sit on top of the ZF plate to maintain the temperature within the plate at 28.5 degrees.

**Data analysis and quantification**

Quantification of GEDI and morphology channel fluorescence intensity from 2D cultures was done using files obtained by automated imaging as previously described[3,14,102]. Files were processed using custom scripts running within a custom built image processing Galaxy bioinformatics cluster[25,103] that background subtracts, montages, fine tunes alignment across time points of imaging, segments individual neurons, tracks segmented neurons over time and then extracts intensity and feature information from each neuron into a csv file. Background subtraction was performed by subtracting the median intensity of each image, and was required for calculation of a translatable GEDI signal across data sets. Segmentation of neurons was targeted towards detection of the brightest area of the morphology of the neuron, usually the soma, that was larger than a minimal size threshold of 100 pixels. The GEDI ratio is sensitive to extent of segmentation of neurons, and errors in segmentation that include background can reduce the precision of the GEDI ratio obtained. A tight segmentation of neurons around the soma is desirable as segmentation of neurites frequently results in segmentation of multiple neurons at a time because of overlapping projections, and the dimmer and inconsistent morphology fluorescence signal extension throughout neurites. Tracking of neurons was performed by labeling an object as the same object at the next time point based on the proximity of the coordinates of the segmented mask to a segmented mask at the previous time point. Survival analysis was performed by defining the time of death as the point at which the GEDI ratio of a longitudinally imaged neuron exceeds the empirically calculated GEDI threshold, or

the point at which point a tracked segmentation label is lost, which was performed using custom scripts written in R. The GEDI threshold was determined using the following equation:

(1) *GEDI ratio threshold= ([(mean GEDI ratio dead)-(mean GEDI ratio live)]*0.25) + [mean GEDI ratio live]*

The survival package for R statistical software was used to construct Kaplan–Meier curves from the survival data based on GEDI ratio, and survival functions were fit to these curves to derive cumulative survival and risk-of-death curves that describe the instantaneous risk of death for individual neurons as previously described[39]. Linear regressions of log decay and nonlinear regressions of GEDI signal increase were calculated in Prism using plateau followed by one phase association kinetics.

For zebrafish motor axon area quantification, *in toto* z-stacks of immobilized fish were maximum projected, stitched together, background subtracted, and binarized. The spinal cord soma, brain and eye fluorescence typical of *mnx1* transgenics[66] was manually masked out using FIJI, leaving only the motor axon projections and the total area of signal was quantified per fish and standardized to the initial time point for that fish. For zebrafish analysis of GEDI signal, *in toto* z-stacks of immobilized fish were stitched together, background subtracted per z plane, and all imaging channels over time were combined into a 5D composite hyperstacks (x, y, z, color, and time dimensions). Due to a spherical aberration commonly present in confocal 3D imaging and present on this platform[25,104], maximum projections across z planes created blurry images that limited precision in quantification, so individual z planes were used for all fluorescence quantifications of GCaMP 7and GEDI. In Tg:mnx1:GCaMP7/NTR-mCherry experiments, GEDI ratio was calculated per hemi-segment because individual neurons could not be easily resolved.

In neuroD:NTR-BFP experiments, individual neurons were located by the co-expression of the GEDI morphology channel with the NTR-BFP while blinded to the GEDI fluorescence.

**iPSC Differentiation to MNs**

iPSC line derived from a healthy control individual (KW4) was obtained from the Yamanaka lab[97]. A line containing the SOD1 D90A mutation was acquired from the iPSC repository at the the Packard Center at Johns Hopkins. Reprogramming and characterization of the SOD1 D90 iPSC line were previously reported[105]. Healthy and SOD1 D90A iPSCs were found to be karyotypically normal, and were differentiated into MNs using a modified dual-SMAD inhibition protocol[106] (http://neurolincs.org/pdf/diMN-protocol.pdf). At day 18 of differentiation, iPSC-derived MNs were dissociated using trypsin (Thermo Fisher), embedded in diluted Matrigel (Corning) to limit cell motility, and plated onto Matrigel-coated 96-well plates. From day 20–35, the neurons underwent a medium change every 2-3 days.

**Figure 1. GEDI detects death of neurons.**

A) Relative fluorescence of GECI's GCaMP6f[79] and RCEPIA[37]/RGEDI across $Ca^{2+}$ concentrations present in the cytosol, endoplasmic reticulum, and extracellular milieu modeled from previously reported Hill coefficients and $K_d$ values. B) Representative fluorescence images of rat primary cortical neurons transfected with GCaMP6f or RGEDI at baseline, during 30 Hz*3s field stimulation, or after 2% $NaN_3$ treatment, scale= 10µm. C,D) Representative trace of time course of standardized ΔF/F fluorescence after 30 Hz*3s stimulation (open arrowhead), and after $NaN_3$ treatment (black arrowhead) of GCaMP6f (C) and RGEDI (D) expressing neurons. E) To determine whether RGEDI signals were specific for cell death and not confounded by

physiological $Ca^{2+}$ transients, the ratio of the maximum signal from electrical stimulation to toxin treatment per neuron are shown, demonstrating that GEDI does not respond to physiological $Ca^{2+}$ transients (*** T test, $p<0.0001$). Error bars represent SEM. F) Design of RGEDI-P2a-EGFP cassette for pseudo-ratiometric expression in neurons. G) Illustration of color change in red:green image overlay expected in a live versus dead neuron. Live neurons have EGFP (green) and basal RGEDI (red) fluorescence (overlaid as yellow) within the soma of the neuron, surrounded by green fluorescence that expands through the neurites. Dead neurons display yellow fluorescence throughout, with edges of red fluorescence around the soma and throughout degenerating neurites as extracellular $Ca^{2+}$ permeates the membrane (arrows). H) Time course images of rat primary cortical neurons expressing RGEDI-P2a-EGFP at 24–36 hours post transfection. Neuron 1 shows characteristic morphology features of death followed by loss of fluorescence at 36 hours post transfection while Neuron 2 remains alive, scale= 20µm. I) Quantification of change in GEDI ratio of Neurons 1 and 2 in (H). J) Quantification of GEDI ratio in rat primary cortical neurons before and 5 minutes after $NaN_3$-induced neuronal death. Dotted line represents calculated GEDI threshold. (*** One-tailed T test $p<0.0001$). K) Quantification and classification of death in neuronal cultures at 24 and 48 hours after co-transfection of RGEDI-P2a-EGFP and an N-terminal exon 1 fragment of Huntingtin, the protein that causes Huntington's disease, with a disease-associated expansion of the polyglutamine stretch (HttEx1Q97) to induce neuronal death using the derived GEDI threshold from (J) to define death. Independently, neurons were scored as dead (red), or live (green) by eye using EGFP at 24, 48, and 72 post transfection. Neurons that were classified as live by eye but above the GEDI threshold and classified as dead at the subsequent timepoint were called human errors (black).

**Figure 2. Detection and characterization of subpopulations of neurons resistant or sensitive to glutamate treatment using GEDI.**

A) Representative two color overlay image from a well of rat primary cortical neurons expressing RGEDI-P2a-EGFP before treatment with 0.1 mM glutamate (Scale = 400 μm) and zoom-in of two individual neurons within the yellow box (Scale = 100 μm). Live neurons appear green/yellow, dead neurons appear yellow/red. B) Representative two color overlay image from neurons 3 hours after treatment with 1mM glutamate and enlargement of the same two neurons within the yellow box in (A). C) Time course images of a neuron before and after exposure to 0.1mM glutamate that survives until 96 hours post-treatment (Scale = 50 μm). D) Kaplan-Meyer plot of neuron survival after exposure to 1mM, 0.1mM, 0.01mM and 0 glutamate (n=699, 585, 527, 476). E) Linear regressions of decay of EGFP (left) and RGEDI (right) after neuronal death marked by GEDI signal above the threshold . F) Slopes of decay of EGFP and RGEDI signals are not different (Mann-Whitney, ns= not significant, p=0.93, n=5513). Horizontal lines in violin plot represent quartiles and median.

**Figure 3. Detection of death in neurodegenerative disease models with GEDI**

A) Representative two-color overlay images of rat primary cortical neuron at 24 and 48 hours after transfection co-expressing RGEDI-P2a-EGFP and HttEx1Q97 (A'), α-synuclein (A''), or TDP43 (A'''). The GEDI ratio identifies each neuron as live at 24, but dead at 48 hours post transfection. Scale= 25μm. B) Quantification of GEDI ratio during longitudinal imaging across 168 hours of live culture of neurons expressing HttEx1Q97 (B), α-synuclein (B'), or TDP43 (B'') with GEDI thresholds at 0.05 for each data set. Dots are color coded for time post imaging.

C) Cumulative risk-of-death of HttEx1Q97 (HR= 1.83, 95% CI= 1.67-2.01, * $p<0.001$), HttEx1Q25 (HR=1.07, 95% CI=0.99-1.15, ns, not significant p=0.08), α-synuclein (HR=1.73, 95% CI= 1.58-1.89, * $p<0.001$), TDP43 (HR=1.77, 95% CI=1.6-1.94, * $p<0.001$), and RGEDI-P2a-EGFP alone (control) generated from GEDI ratio quantification and classification against the GEDI threshold. Number of neurons in Control= 1670, HttEx1Q25-CFP = 1333, HttEx1Q97-CFP = 668, TDP43= 610, and α-synuclein =743. D) Representative time lapse imaging of a control iPSC motor neuron expressing RGEDI-P2a-EGFP that survives throughout imaging. E) Representative time lapse imaging of a SOD1 D90A iPSC motor neuron that is dead by GEDI signal at 84 hours of after transfection. F) Quantification of the GEDI ratio of Control and SOD1 D90A neurons and the derived GEDI threshold at 0.05. G) CRD plot of SOD1-D90A and Control (95% CI= 1.11-1.44, $p<0.0001$, number of neurons in Control= 714, and SOD1 D90A=363).

**Figure 4. Comparison of GEDI variants to detect neuronal death**

A–C) Representative images of rat primary cortical neurons expressing RGEDI-P2a-3xBFP (A), mRuby-P2a-GCaMP6f (B), or RGEDI-P2a-EGFP (C), before, 5 minutes, and 10 minutes after exposure to $NaN_3$. D) Quantification and non-linear regressions of increases in fluorescence signals over time from variants of the GEDI biosensor: RGEDI-P2a-3xBFP (n=23), mRuby-P2a-GCaMP6f (n=52), RGEDI-P2a-EGFP (n=41), GC150-P2a-mApple, RGEDI-NLS-P2a-EGFP-NLS, and GC150-NLS-P2a-mApple-NLS (n=40). E) Relative fluorescence of GECI's GCaMP6f[79] and RCEPIA[37]/RGEDI and GCaMP150ER[38]/GC150 across $Ca^{2+}$ concentrations modeled from previously reported Hill coefficients and $K_d$ values. (F) Representative images of rat primary cortical neurons expressing GC150-P2a-mApple, (G) GC150-NLS-P2a-mApple-

NLS and (H) RGEDI-NLS-P2a-EGFP-NLS before, 5 minutes, and 10 minutes after exposure to $NaN_3$. Error bars represent SEM. Scale= 25µm.

**Figure 5. Acute detection of death in live zebrafish using GCaMP7**

A) *in toto* confocal imaging of UAS:EGFP labeled MNs within live, 72 hpf, immobilized zebrafish larvae beginning at 0, 24 or 48 hours after DMSO (left) or 10 µM MTZ exposure (right). Yellow arrow and asterisk indicate developing and intact motor axons and somas respectively, red arrow and asterisk indicate degenerating motor axons, and somas respectively. Scale = 100µm. B) Zoom-in of MNs from (A) exposed to DMSO (top) or MTZ (bottom). Scale = 100µm. C) Quantification of % change of motor axon area per fish after treatment with DMSO (n=7) or MTZ (n=15) (ns, not significant; **** T Test p<0.0001). D) Traces of touch-evoked swimming behavior from 96hpf larvae after 24 hours of DMSO or 10 µM MTZ treatment. Each fish swimming trace is labeled with a different color and a dot per second. E) Quantification of average velocity of 96hpf larvae touch evoked swimming at 1 hours and 24 hours (n= 358)(F) after DMSO (n= 438) or 10 µM MTZ treatment (n=312), or untreated larvae expressing UAS:BoTx-EGFP in MNs (n=301) (one-sided Kruskal-Wallis test, ns= not significant; **** p<0.0001). G) Magnification of MNs from *in toto* confocal imaging of transgenic UAS:NTR-mCherry;UAS:GCaMP7 live immobilized larvae at 0, 24 or 48 hours after DMSO or (H) 10µM MTZ exposure showing increase in GCaMP7 signal in MTZ treated neurons. I) Quantification of mean GCaMP/ mCherry ratio per fish from (F) for DMSO (at 0, 24, 48, 72 hours post treatment n = 6, 6, 5, 2) and MTZ treatments (at 0, 24, 48, 72 hours post treatment n = 9, 8, 8, 7) (ns, not significant; ANOVA Sidak's, **** p<0.0001, ** p<0.01). Error bars represent SEM.

**Figure 6 Single cell tracking and specific detection of death *in vivo* within live zebrafish larvae with GC150 but not RGEDI**

A) Cartoon schematic of zebrafish larvae showing approximate location of sparsely labeled clusters of neurons. B) Neurons in the zebrafish larvae spinal cord co-expressing NTR-BFP, EGFP, and RGEDI at 0, 24, and 48 hours after mounting for automated imaging in MTZ. White arrows indicate neurons co-expressing NTR-BFP and EGFP. Scale= 50µm. C) Quantification of GEDI ratio in neurons co-expressing NTR-BFP and RGEDI-P2a-EGFP exposed to MTZ (n=7) or DMSO (n= 5) showing no increase in GEDI signal (ANOVA Sidak's, ns= not significant). D) Neurons in the zebrafish larvae spinal cord co-expressing NTR-BFP, mApple, and GC150 at 0, 24, and 48 hours after mounting for automated imaging in DMSO. White arrows indicate neurons with fluorescence of BFP and mApple, asterisks indicate autofluorescence from pigment in larvae skin, scale= 20µm. E) Quantification of average GEDI ratio of neurons from zebrafish larvae incubated in DMSO (n= 7) or 10µM MTZ (n=17) over time showing increase in GEDI ratio in neurons indicating neuronal death after 24 hours in MTZ (ANOVA Tukey's ****= $p<0.0001$, *** = $p<0.0005$). F) Neurons in zebrafish larvae spinal cord co-expressing NTR-BFP, mApple, and GC150 at 0, 24, and 48 hours after mounting for automated imaging in 10µM MTZ. White arrows indicate neurons with fluorescence of BFP and mApple, yellow arrows indicate neurons with fluorescence of BFP, mApple, and GC150, indicating neuronal death. Asterisks indicates autofluorescence from pigment in larvae skin, scale= 20µm. Error bars represent SEM.

## AUTHOR CONTRIBUTIONS

JL and SF wrote the manuscript. JL, KS, NC, and SF designed the automatic microscopy experiments. Molecular biology, biosensor design, and rodent primary neuron culturing and imaging performed by JL. JL and DK designed zebrafish experiments. JL and VO performed zebrafish microinjections and imaging experiments, JL and MM performed zebrafish behavior experiments. NC and MC carried out death delay experiments with dyes and GEDI. DH performed stimulation and imaging experiments. KS performed iPS differentiation, culturing, transfection and imaging experiments. Custom scripts for analysis of imaging experiments done by JL and KS. All authors reviewed the manuscript**.**

### Code Availability

The code is copyright protected, and its use in performing the described research is patented (U.S. Patent 7,139,415 and U.S. Patent Application 14/737,325). Code is available upon request to the corresponding author. Access to and use of the code is subject to a non-exclusive, revocable, non-transferable, and limited right to use the code for the exclusive purpose of undertaking academic, governmental, or not-for- profit research. Use of the code or any part thereof for commercial or clinical purposes is strictly prohibited in the absence of a Commercial License Agreement from The J. David Gladstone Institutes.

## DATA AVAILABILITY

The data that support the findings of this study are available from the corresponding author upon reasonable request.

## COMPETING INTERESTS

The Authors declare no Competing Non-Financial Interests, but the following Competing Financial Interests: SMF is the inventor of Robotic Microscopy Systems, U.S. Patent 7,139,415 and Automated Robotic Microscopy Systems, U.S. Patent Application 14/737,325, both assigned to The J. David Gladstone Institutes. A provisional US and EPO patent for the GEDI biosensor (inventors Jeremy Linsley, Kevan Shah, and Steve Finkbeiner) assigned to The J. David Gladstone Institutes has been placed GL2016-815, May 2019.

**Acknowledgements—** This work was supported by grants from the NIH (U54 NS191046, R37 NS101996, RF1 AG058476, RF1 AG056151, RF1 AG058447, P01 AG054407, U01 MH115747), as well as support from the Koret Foundation Artificial Intelligence Program for Biomedical Research and the Taube/Koret Center for Neurodegenerative Disease Research. The Gladstone Institutes received support from a National Center for Research Resources Grant RR18928. We gratefully acknowledge the support of NVIDIA Corporation with the donation of the Titan Xp GPU used for this research. Kathryn Claiborn provided editorial assistance, Kelley Nelson and Gayane Abramova administrative assistance, Cailtyn Bonilla helped troubleshoot the microscope, and David Cahill provided lab maintenance and organization. Elliot Mount provided key assistance in configuring and troubleshooting the microscope to image live zebrafish. Mnx1 plasmid and transgenic zebrafish line were kind gift from E. Isakoff (UC-Berkeley). Jack Taylor, Matthew Mccarroll, Louie Ramos and Ethan Fertsch (UCSF) and Claire Quinata (Gladstone Institutes) provided zebrafish expertise and colony maintenance. We thank Ken Nakamura for the use of field stimulation and imaging equipment, helpful comments and support. Sean Low

(University of Michigan) provided zebrafish expertise, mentoring, guidance, and calcium imaging assistance.

## REFERENCES


1. Skibinski G, Hwang V, Ando DM, et al. Nrf2 mitigates LRRK2- and α-synuclein–induced neurodegeneration by modulating proteostasis. *Proc Natl Acad Sci U S A.* 2016;114(5):1165–1170.
2. Skibinski G, Nakamura K, Cookson MR, Finkbeiner S. Mutant LRRK2 toxicity in neurons depends on LRRK2 levels and synuclein but not kinase activity or inclusion bodies. *J Neurosci* 2014;34(2):418-433.
3. Arrasate M, Mitra S, Schweitzer ES, Segal MR, Finkbeiner S. Inclusion body formation reduces levels of mutant huntingtin and the risk of neuronal death. *Nature.* 2004;431(7010):805-810.
4. Miller J, Arrasate M, Brooks E, et al. Identifying polyglutamine protein species in situ that best predict neurodegeneration. *Nat Chem Biol* 2011;7(12):925–934.
5. Miller J, Arrasate M, Shaby BA, Mitra S, Masliah E, Finkbeiner S. Quantitative relationships between huntingtin levels, polyglutamine length, inclusion body formation, and neuronal death provide novel insight into huntington's disease molecular pathogenesis. *J Neurosci.* 2010;30(31):10541–10550.
6. Tsvetkov AS, Arrasate M, Barmada S, et al. Proteostasis of polyglutamine varies among neurons and predicts neurodegeneration. *Nat Chem Biol* 2013;9(9):586–592.
7. Tsvetkov AS, Miller J, Arrasate M, Wong JS, Pleiss MA, Finkbeiner S. A small-molecule scaffold induces autophagy in primary neurons and protects against toxicity in a Huntington disease model. *Proc Natl Acad Sci U S A* 2010;107(39):16982–16987.
8. Barmada SJ, Serio A, Arjun A, et al. Autophagy induction enhances TDP43 turnover and survival in neuronal ALS models. *Nat Chem Biol.* 2014;10(8):677–685.
9. Barmada SJ, Skibinski G, Korb E, Rao EJ, Wu JY, Finkbeiner S. Cytoplasmic mislocalization of TDP-43 is toxic to neurons and enhanced by a mutation associated with familial amyotrophic lateral sclerosis. *J Neurosci* 2010;30(2):639–649.
10. Surmeier DJ, Obeso JA, Halliday GM. Selective neuronal vulnerability in Parkinson disease. *Nat Rev Neurosci.* 2017;18(2):101–113.
11. Rodrigue KM, Rieck JR, Kennedy KM, Devous MD, Sr., Diaz-Arrastia R, Park DC. Risk factors for beta-amyloid deposition in healthy aging: vascular and genetic effects. *JAMA Neurol.* 2013;70(5):600-606.
12. Linsley JW, Reisine T, Finkbeiner S. Cell death assays for neurodegenerative disease drug discovery. *Expert Opinion on Drug Discovery.* 2019:1-13.
13. Kepp O, Galluzzi L, Lipinski M, Yuan J, Kroemer G. Cell death assays for drug discovery. *Nature reviews Drug discovery.* 2011;10(3):221-237.
14. Arrasate M, Finkbeiner S. Automated microscope system for determining factors that predict neuronal fate. *Proc Natl Acad Sci U S A.* 2005;102(10):3840–3845.
15. Finkbeiner S, Frumkin M, Kassner PD. Cell-based screening: Extracting meaning from complex data. *Neuron.* 2015;86(1):160–174.
16. Guo F, Liu X, Cai H, Le W. Autophagy in neurodegenerative diseases: pathogenesis and therapy. *Brain pathology (Zurich, Switzerland).* 2018;28(1):3-13.
17. Riss TL MR, Niles AL, et al. Cell Viability Assays. *Eli Lilly & Company and the National Center for Advancing Translational Sciences.* 2016;Jul 1.

18. van Ham TJ, Mapes J, Kokel D, Peterson RT. Live imaging of apoptotic cells in zebrafish. *FASEB journal : official publication of the Federation of American Societies for Experimental Biology.* 2010;24(11):4336-4342.
19. Zhang J, Wang X, Cui W, et al. Visualization of caspase-3-like activity in cells using a genetically encoded fluorescent biosensor activated by protein cleavage. *Nature communications.* 2013;4:2157.
20. Gorman AM. Neuronal cell death in neurodegenerative diseases: recurring themes around protein handling. *Journal of cellular and molecular medicine.* 2008;12(6a):2263-2280.
21. Galluzzi L, Vitale I, Aaronson SA, et al. Molecular mechanisms of cell death: recommendations of the Nomenclature Committee on Cell Death 2018. *Cell death and differentiation.* 2018;25(3):486-541.
22. Tucker B, Lardelli M. A rapid apoptosis assay measuring relative acridine orange fluorescence in zebrafish embryos. *Zebrafish.* 2007;4(2):113-116.
23. Horstick EJ, Tabor KM, Jordan DC, Burgess HA. Genetic Ablation, Sensitization, and Isolation of Neurons Using Nitroreductase and Tetrodotoxin-Insensitive Channels. *Methods in molecular biology (Clifton, NJ).* 2016;1451:355-366.
24. Abdelilah S, Mountcastle-Shah E, Harvey M, et al. Mutations affecting neural survival in the zebrafish Danio rerio. *Development (Cambridge, England).* 1996;123:217-227.
25. Linsley JW, Tripathi A, Epstein I, et al. Automated four-dimensional long term imaging enables single cell tracking within organotypic brain slices to study neurodevelopment and degeneration. *Communications biology.* 2019;2:155.
26. Finkbeiner S, Frumkin M, Kassner PD. Cell-based screening: extracting meaning from complex data. *Neuron.* 2015;86(1):160-174.
27. Miyawaki A, Llopis J, Heim R, et al. Fluorescent indicators for Ca2+ based on green fluorescent proteins and calmodulin. *Nature.* 1997;388(6645):882-887.
28. Nagai T, Sawano A, Park ES, Miyawaki A. Circularly permuted green fluorescent proteins engineered to sense Ca2+. *Proceedings of the National Academy of Sciences of the United States of America.* 2001;98(6):3197-3202.
29. Rose T, Goltstein PM, Portugues R, Griesbeck O. Putting a finishing touch on GECIs. *Frontiers in molecular neuroscience.* 2014;7:88.
30. Lin MZ, Schnitzer MJ. Genetically encoded indicators of neuronal activity. *Nature neuroscience.* 2016;19(9):1142-1153.
31. Tominaga K, Geusz ME, Michel S, Inouye ST. Calcium imaging in organotypic cultures of the rat suprachiasmatic nucleus. *Neuroreport.* 1994;5(15):1901-1905.
32. Ahrens MB, Huang KH, Narayan S, Mensh BD, Engert F. Two-photon calcium imaging during fictive navigation in virtual environments. *Frontiers in neural circuits.* 2013;7:104.
33. Huang K, Rupprecht, P., Schebesta, M., Serluca, F., Kitamura, K., Bouwmeester, T., Friedrich, RW. Predictive neural processing in adult zebrafish depends on shank3b. *bioRXiv.* 2019.
34. Sheintuch L, Rubin A, Brande-Eilat N, et al. Tracking the Same Neurons across Multiple Days in Ca(2+) Imaging Data. *Cell reports.* 2017;21(4):1102-1115.
35. Kim DH, Kim J, Marques JC, et al. Pan-neuronal calcium imaging with cellular resolution in freely swimming zebrafish. *Nature methods.* 2017;14(11):1107-1114.
36. Zhao Y, Araki S, Wu J, et al. An expanded palette of genetically encoded Ca(2)(+) indicators. *Science (New York, NY).* 2011;333(6051):1888-1891.

37. Suzuki J, Kanemaru K, Ishii K, Ohkura M, Okubo Y, Iino M. Imaging intraorganellar Ca2+ at subcellular resolution using CEPIA. *Nature communications.* 2014;5:4153.
38. de Juan-Sanz J, Holt GT, Schreiter ER, de Juan F, Kim DS, Ryan TA. Axonal Endoplasmic Reticulum Ca(2+) Content Controls Release Probability in CNS Nerve Terminals. *Neuron.* 2017;93(4):867-881.e866.
39. Skibinski G, Hwang V, Ando DM, et al. Nrf2 mitigates LRRK2- and alpha-synuclein-induced neurodegeneration by modulating proteostasis. *Proceedings of the National Academy of Sciences of the United States of America.* 2017;114(5):1165-1170.
40. Nakamura K, Nemani VM, Azarbal F, et al. Direct membrane association drives mitochondrial fission by the Parkinson disease-associated protein alpha-synuclein. *The Journal of biological chemistry.* 2011;286(23):20710-20726.
41. Merrilees MJ, Beaumont BW, Scott LJ. Fluoroprobe quantification of viable and non-viable cells in human coronary and internal thoracic arteries sampled at autopsy. *Journal of vascular research.* 1995;32(6):371-377.
42. Crissman HA, Steinkamp JA. Rapid, simultaneous measurement of DNA, protein, and cell volume in single cells from large mammalian cell populations. *The Journal of cell biology.* 1973;59(3):766-771.
43. Zhou Y, Danbolt NC. Glutamate as a neurotransmitter in the healthy brain. *Journal of neural transmission (Vienna, Austria : 1996).* 2014;121(8):799-817.
44. Lewerenz J, Maher P. Chronic Glutamate Toxicity in Neurodegenerative Diseases-What is the Evidence? *Frontiers in neuroscience.* 2015;9:469.
45. Fujikawa DG. The role of excitotoxic programmed necrosis in acute brain injury. *Computational and structural biotechnology journal.* 2015;13:212-221.
46. Zhou C, Zhong W, Zhou J, et al. Monitoring autophagic flux by an improved tandem fluorescent-tagged LC3 (mTagRFP-mWasabi-LC3) reveals that high-dose rapamycin impairs autophagic flux in cancer cells. *Autophagy.* 2012;8(8):1215-1226.
47. Huang CJ, Gurlo T, Haataja L, et al. Calcium-activated calpain-2 is a mediator of beta cell dysfunction and apoptosis in type 2 diabetes. *The Journal of biological chemistry.* 2010;285(1):339-348.
48. Chi H, Chang HY, Sang TK. Neuronal Cell Death Mechanisms in Major Neurodegenerative Diseases. *International journal of molecular sciences.* 2018;19(10).
49. Barmada SJ, Ju S, Arjun A, et al. Amelioration of toxicity in neuronal models of amyotrophic lateral sclerosis by hUPF1. *Proceedings of the National Academy of Sciences of the United States of America.* 2015;112(25):7821-7826.
50. Sawa A, Tomoda T, Bae BI. Mechanisms of neuronal cell death in Huntington's disease. *Cytogenetic and genome research.* 2003;100(1-4):287-295.
51. Morrice JR, Gregory-Evans CY, Shaw CA. Necroptosis in amyotrophic lateral sclerosis and other neurological disorders. *Biochimica et biophysica acta Molecular basis of disease.* 2017;1863(2):347-353.
52. Kostrzewa RM. Review of apoptosis vs. necrosis of substantia nigra pars compacta in Parkinson's disease. *Neurotoxicity research.* 2000;2(2-3):239-250.
53. Venderova K, Park DS. Programmed cell death in Parkinson's disease. *Cold Spring Harbor perspectives in medicine.* 2012;2(8).
54. Jager KJ, van Dijk PC, Zoccali C, Dekker FW. The analysis of survival data: the Kaplan-Meier method. *Kidney international.* 2008;74(5):560-565.

55. Haston KM, Finkbeiner S. Clinical trials in a dish: The potential of pluripotent stem cells to develop therapies for Neurodegenerative diseases. *Annu Rev Pharmacol Toxicol.* 2016;56(1):489–510.
56. Luigetti M, Conte A, Madia F, et al. Heterozygous SOD1 D90A mutation presenting as slowly progressive predominant upper motor neuron amyotrophic lateral sclerosis. *Neurological sciences : official journal of the Italian Neurological Society and of the Italian Society of Clinical Neurophysiology.* 2009;30(6):517-520.
57. Chen H, Qian K, Du Z, et al. Modeling ALS with iPSCs reveals that mutant SOD1 misregulates neurofilament balance in motor neurons. *Cell stem cell.* 2014;14(6):796-809.
58. Rose T, Jaepel J, Hubener M, Bonhoeffer T. Cell-specific restoration of stimulus preference after monocular deprivation in the visual cortex. *Science (New York, NY).* 2016;352(6291):1319-1322.
59. Kim CK, Miri A, Leung LC, et al. Prolonged, brain-wide expression of nuclear-localized GCaMP3 for functional circuit mapping. *Frontiers in neural circuits.* 2014;8:138.
60. Martin-Jimenez R, Campanella M, Russell C. New zebrafish models of neurodegeneration. *Current neurology and neuroscience reports.* 2015;15(6):33.
61. Saleem S, Kannan RR. Zebrafish: an emerging real-time model system to study Alzheimer's disease and neurospecific drug discovery. *Cell death discovery.* 2018;4:45.
62. Xu J, Wang T, Wu Y, Jin W, Wen Z. Microglia Colonization of Developing Zebrafish Midbrain Is Promoted by Apoptotic Neuron and Lysophosphatidylcholine. *Developmental cell.* 2016;38(2):214-222.
63. Fett ME, Pilsl A, Paquet D, et al. Parkin is protective against proteotoxic stress in a transgenic zebrafish model. *PloS one.* 2010;5(7):e11783.
64. Pyati UJ, Look AT, Hammerschmidt M. Zebrafish as a powerful vertebrate model system for in vivo studies of cell death. *Seminars in cancer biology.* 2007;17(2):154-165.
65. Curado S, Stainier DY, Anderson RM. Nitroreductase-mediated cell/tissue ablation in zebrafish: a spatially and temporally controlled ablation method with applications in developmental and regeneration studies. *Nature protocols.* 2008;3(6):948-954.
66. Zelenchuk TA, Bruses JL. In vivo labeling of zebrafish motor neurons using an mnx1 enhancer and Gal4/UAS. *Genesis (New York, NY : 2000).* 2011;49(7):546-554.
67. Sternberg JR, Severi KE, Fidelin K, et al. Optimization of a Neurotoxin to Investigate the Contribution of Excitatory Interneurons to Speed Modulation In Vivo. *Current biology : CB.* 2016;26(17):2319-2328.
68. Tabor KM, Bergeron SA, Horstick EJ, et al. Direct activation of the Mauthner cell by electric field pulses drives ultrarapid escape responses. *Journal of neurophysiology.* 2014;112(4):834-844.
69. Muto A, Ohkura M, Kotani T, Higashijima S, Nakai J, Kawakami K. Genetic visualization with an improved GCaMP calcium indicator reveals spatiotemporal activation of the spinal motor neurons in zebrafish. *Proceedings of the National Academy of Sciences of the United States of America.* 2011;108(13):5425-5430.
70. Attili S, Hughes SM. Anaesthetic tricaine acts preferentially on neural voltage-gated sodium channels and fails to block directly evoked muscle contraction. *PloS one.* 2014;9(8):e103751.
71. Lopez-Luna J, Al-Jubouri Q, Al-Nuaimy W, Sneddon LU. Impact of stress, fear and anxiety on the nociceptive responses of larval zebrafish. *PloS one.* 2017;12(8):e0181010.

72. Cheung A, Dantzig JA, Hollingworth S, et al. A small-molecule inhibitor of skeletal muscle myosin II. *Nature cell biology.* 2002;4(1):83-88.
73. Zhou W, Saint-Amant L, Hirata H, Cui WW, Sprague SM, Kuwada JY. Non-sense mutations in the dihydropyridine receptor beta1 gene, CACNB1, paralyze zebrafish relaxed mutants. *Cell calcium.* 2006;39(3):227-236.
74. Zahl IH, Samuelsen O, Kiessling A. Anaesthesia of farmed fish: implications for welfare. *Fish physiology and biochemistry.* 2012;38(1):201-218.
75. Kanai K, Shibuya K, Sato Y, et al. Motor axonal excitability properties are strong predictors for survival in amyotrophic lateral sclerosis. *J Neurol Neurosurg Psychiatry.* 2012;83(7):734–738.
76. Vossel KA, Beagle AJ, Rabinovici GD, et al. Seizures and epileptiform activity in the early stages of Alzheimer disease. *JAMA Neurol.* 2013;70(9):1158.
77. Naumann EA, Kampff AR, Prober DA, Schier AF, Engert F. Monitoring neural activity with bioluminescence during natural behavior. *Nature neuroscience.* 2010;13(4):513-520.
78. Zhang Y, Chen X, Gueydan C, Han J. Plasma membrane changes during programmed cell deaths. *Cell research.* 2018;28(1):9-21.
79. Chen TW, Wardill TJ, Sun Y, et al. Ultrasensitive fluorescent proteins for imaging neuronal activity. *Nature.* 2013;499(7458):295-300.
80. Reyes RC, Brennan AM, Shen Y, Baldwin Y, Swanson RA. Activation of neuronal NMDA receptors induces superoxide-mediated oxidative stress in neighboring neurons and astrocytes. *The Journal of neuroscience : the official journal of the Society for Neuroscience.* 2012;32(37):12973-12978.
81. Minnella AM, Zhao JX, Jiang X, et al. Excitotoxic superoxide production and neuronal death require both ionotropic and non-ionotropic NMDA receptor signaling. *Scientific reports.* 2018;8(1):17522.
82. Brennan-Minnella AM, Won SJ, Swanson RA. NADPH oxidase-2: linking glucose, acidosis, and excitotoxicity in stroke. *Antioxidants & redox signaling.* 2015;22(2):161-174.
83. Brennan AM, Suh SW, Won SJ, et al. NADPH oxidase is the primary source of superoxide induced by NMDA receptor activation. *Nature neuroscience.* 2009;12(7):857-863.
84. Berridge MJ, Lipp P, Bootman MD. The versatility and universality of calcium signalling. *Nature reviews Molecular cell biology.* 2000;1(1):11-21.
85. Kanai K, Kuwabara S, Misawa S, et al. Altered axonal excitability properties in amyotrophic lateral sclerosis: Impaired potassium channel function related to disease stage. *Brain : a journal of neurology.* 2006;129(4):953–962.
86. Poudel GR, Egan GF, Churchyard A, Chua P, Stout JC, Georgiou-Karistianis N. Abnormal synchrony of resting state networks in premanifest and symptomatic Huntington disease: the IMAGE-HD study. *Journal of psychiatry & neuroscience : JPN.* 2014;39(2):87-96.
87. Jucker M, Walker LC. Self-propagation of pathogenic protein aggregates in neurodegenerative diseases. *Nature.* 2013;501(7465):45-51.
88. Masnata M, Cicchetti F. The Evidence for the Spread and Seeding Capacities of the Mutant Huntingtin Protein in in Vitro Systems and Their Therapeutic Implications. *Frontiers in neuroscience.* 2017;11:647.

89. Jucker M, Walker LC. Pathogenic protein seeding in Alzheimer disease and other neurodegenerative disorders. *Annals of neurology.* 2011;70(4):532-540.
90. Abdelfattah AS, Farhi SL, Zhao Y, et al. A Bright and Fast Red Fluorescent Protein Voltage Indicator That Reports Neuronal Activity in Organotypic Brain Slices. *The Journal of neuroscience : the official journal of the Society for Neuroscience.* 2016;36(8):2458-2472.
91. Pardo-Martin C, Chang TY, Koo BK, Gilleland CL, Wasserman SC, Yanik MF. High-throughput in vivo vertebrate screening. *Nat Methods.* 2010;7(8):634-636.
92. Saint-Amant L, Drapeau P. Time course of the development of motor behaviors in the zebrafish embryo. *Journal of neurobiology.* 1998;37(4):622-632.
93. Kalueff AV, Gebhardt M, Stewart AM, et al. Towards a comprehensive catalog of zebrafish behavior 1.0 and beyond. *Zebrafish.* 2013;10(1):70-86.
94. Ghosh S, Hui SP. Regeneration of Zebrafish CNS: Adult Neurogenesis. *Neural plasticity.* 2016;2016:5815439.
95. Nicholson C, ten Bruggencate G, Stockle H, Steinberg R. Calcium and potassium changes in extracellular microenvironment of cat cerebellar cortex. *Journal of neurophysiology.* 1978;41(4):1026-1039.
96. Egelman DM, Montague PR. Calcium dynamics in the extracellular space of mammalian neural tissue. *Biophysical journal.* 1999;76(4):1856-1867.
97. Christiansen EM, Yang SJ, Ando DM, et al. In silico labeling: Predicting fluorescent labels in unlabeled images. *Cell.* 2018;173(3):792–803.e719.
98. Linsley JW, Hsu IU, Groom L, et al. Congenital myopathy results from misregulation of a muscle Ca2+ channel by mutant Stac3. *Proceedings of the National Academy of Sciences of the United States of America.* 2017;114(2):E228-e236.
99. Kwan KM, Fujimoto E, Grabher C, et al. The Tol2kit: a multisite gateway-based construction kit for Tol2 transposon transgenesis constructs. *Developmental dynamics : an official publication of the American Association of Anatomists.* 2007;236(11):3088-3099.
100. McGraw HF, Snelson CD, Prendergast A, Suli A, Raible DW. Postembryonic neuronal addition in zebrafish dorsal root ganglia is regulated by Notch signaling. *Neural development.* 2012;7:23.
101. Karlsson J, von Hofsten J, Olsson PE. Generating transparent zebrafish: a refined method to improve detection of gene expression during embryonic development. *Marine biotechnology (New York, NY).* 2001;3(6):522-527.
102. Daub A, Sharma P, Finkbeiner S. High-content screening of primary neurons: ready for prime time. *Current opinion in neurobiology.* 2009;19(5):537-543.
103. Afgan E, Baker D, van den Beek M, et al. The Galaxy platform for accessible, reproducible and collaborative biomedical analyses: 2016 update. *Nucleic acids research.* 2016;44(W1):W3-w10.
104. Caster AH, Kahn RA. Computational method for calculating fluorescence intensities within three-dimensional structures in cells. *Cellular logistics.* 2012;2(4):176-188.
105. Li Y, Balasubramanian U, Cohen D, et al. A comprehensive library of familial human amyotrophic lateral sclerosis induced pluripotent stem cells. *PloS one.* 2015;10(3):e0118266.

106. Chambers SM, Fasano CA, Papapetrou EP, Tomishima M, Sadelain M, Studer L. Highly efficient neural conversion of human ES and iPS cells by dual inhibition of SMAD signaling. *Nature biotechnology.* 2009;27(3):275-280.

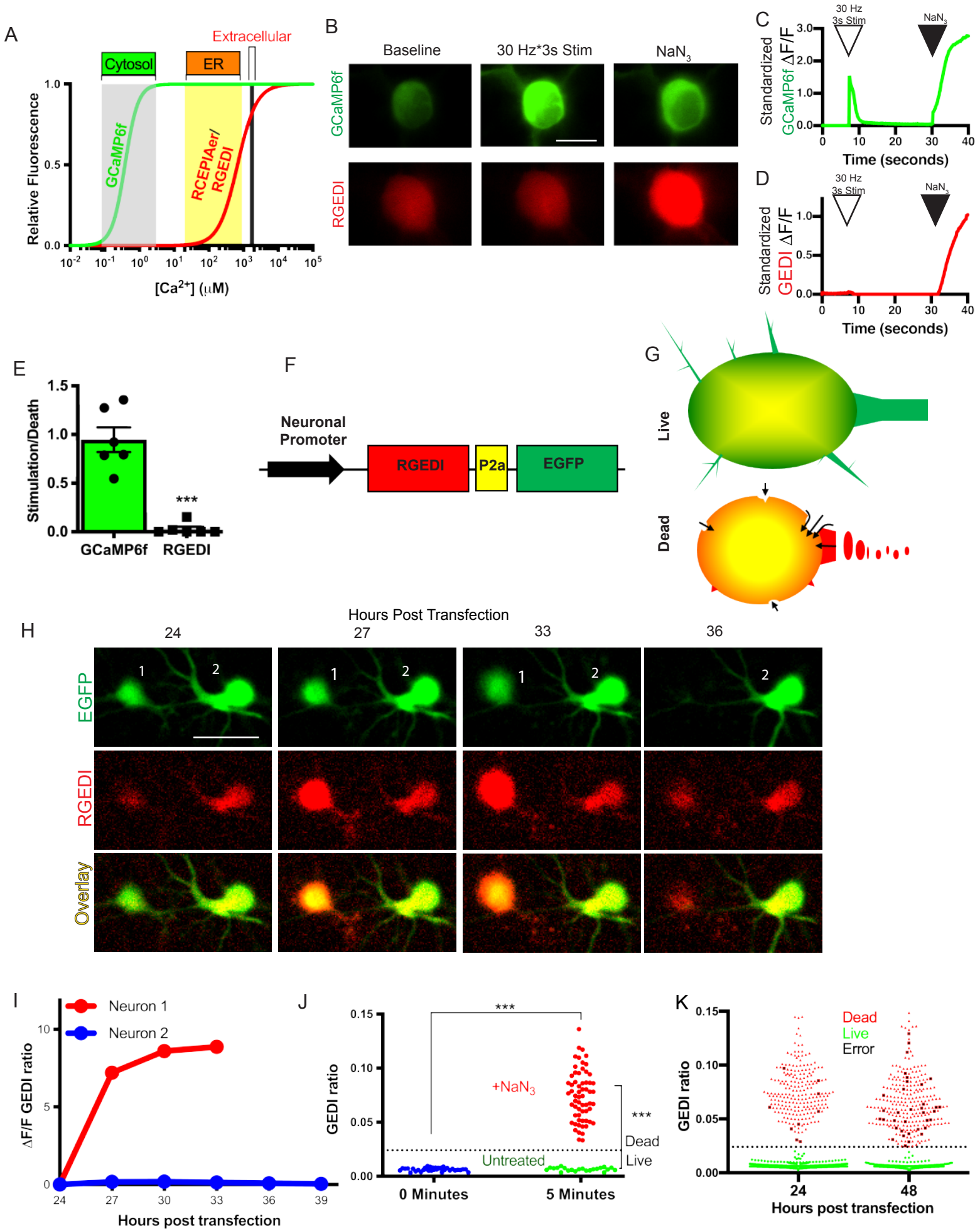
A
Extracellular
Cytosol
ER
Relative Fluorescence
GCaMP6f
RCEPIAer/
RGEDI
[Ca2+] (μM)
B
Baseline
30 Hz*3s Stim
NaN3
GCaMP6f
RGEDI
C
30 Hz
3s Stim
NaN3
Standardized
GCaMP6f ΔF/F
Time (seconds)
D
30 Hz
3s Stim
NaN3
Standardized
GEDI ΔF/F
Time (seconds)
E
Stimulation/Death
***
GCaMP6f
RGEDI
F
Neuronal
Promoter
RGEDI
P2a
EGFP
G
Live
Dead
H
Hours Post Transfection
24
27
33
36
EGFP
RGEDI
Overlay
I
Neuron 1
Neuron 2
ΔF/F GEDI ratio
Hours post transfection
J
***
+NaN3
***
Dead
Live
Untreated
GEDI ratio
0 Minutes
5 Minutes
K
Dead
Live
Error
GEDI ratio
24
48
Hours post transfection

Figure 1

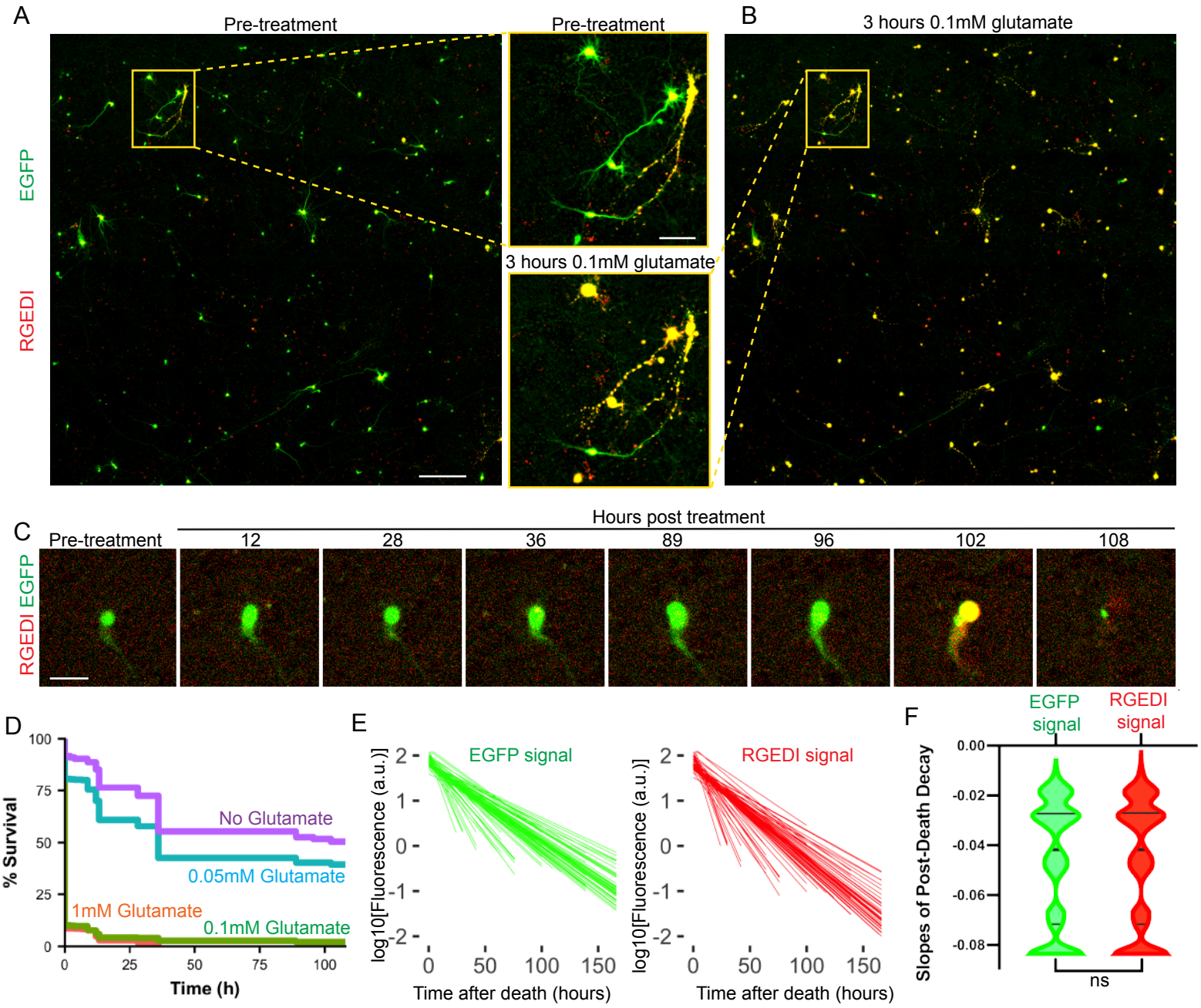
A
Pre-treatment
Pre-treatment
3 hours 0.1mM glutamate
EGFP
RGEDI
B
3 hours 0.1mM glutamate
C
Hours post treatment
Pre-treatment
12
28
36
89
96
102
108
RGEDI EGFP
D
% Survival
Time (h)
No Glutamate
0.05mM Glutamate
1mM Glutamate
0.1mM Glutamate
E
EGFP signal
RGEDI signal
log10[Fluorescence (a.u.)]
Time after death (hours)
F
EGFP signal
RGEDI signal
Slopes of Post-Death Decay
ns

Figure 2

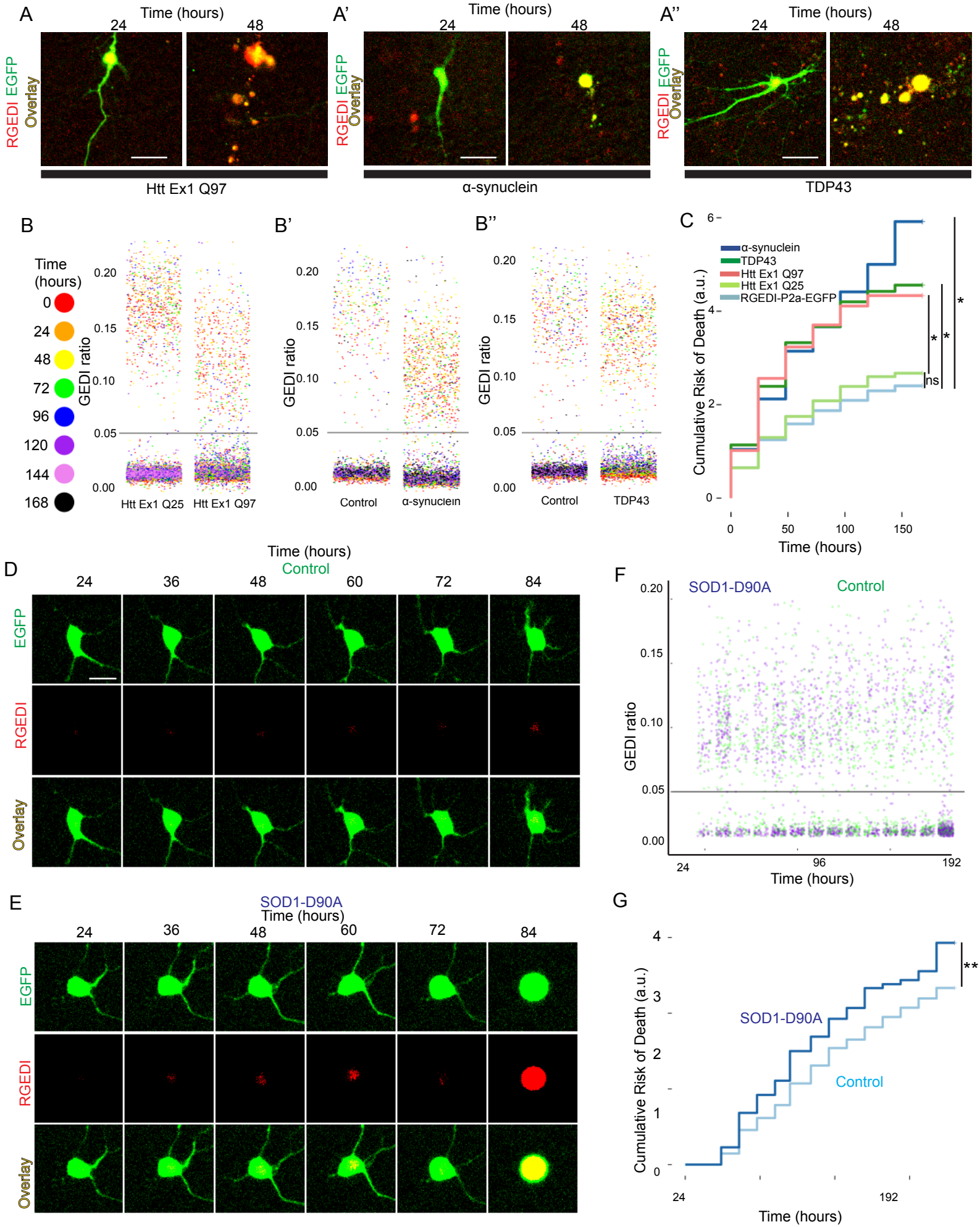
A
Time (hours)
24
48
RGEDI EGFP
Overlay
Htt Ex1 Q97
A'
Time (hours)
24
48
RGEDI EGFP
Overlay
α-synuclein
A''
Time (hours)
24
48
RGEDI EGFP
Overlay
TDP43
B
Time (hours)
0
24
48
72
96
120
144
168
GEDI ratio
0.20
0.15
0.10
0.05
0.00
Htt Ex1 Q25
Htt Ex1 Q97
B'
GEDI ratio
Control
α-synuclein
B''
GEDI ratio
Control
TDP43
C
α-synuclein
TDP43
Htt Ex1 Q97
Htt Ex1 Q25
RGEDI-P2a-EGFP
Cumulative Risk of Death (a.u.)
ns
*
*
*
Time (hours)
D
Time (hours)
Control
24
36
48
60
72
84
EGFP
RGEDI
Overlay
E
SOD1-D90A
Time (hours)
24
36
48
60
72
84
EGFP
RGEDI
Overlay
F
SOD1-D90A
Control
GEDI ratio
Time (hours)
G
SOD1-D90A
Control
Cumulative Risk of Death (a.u.)
**
Time (hours)

Figure 3

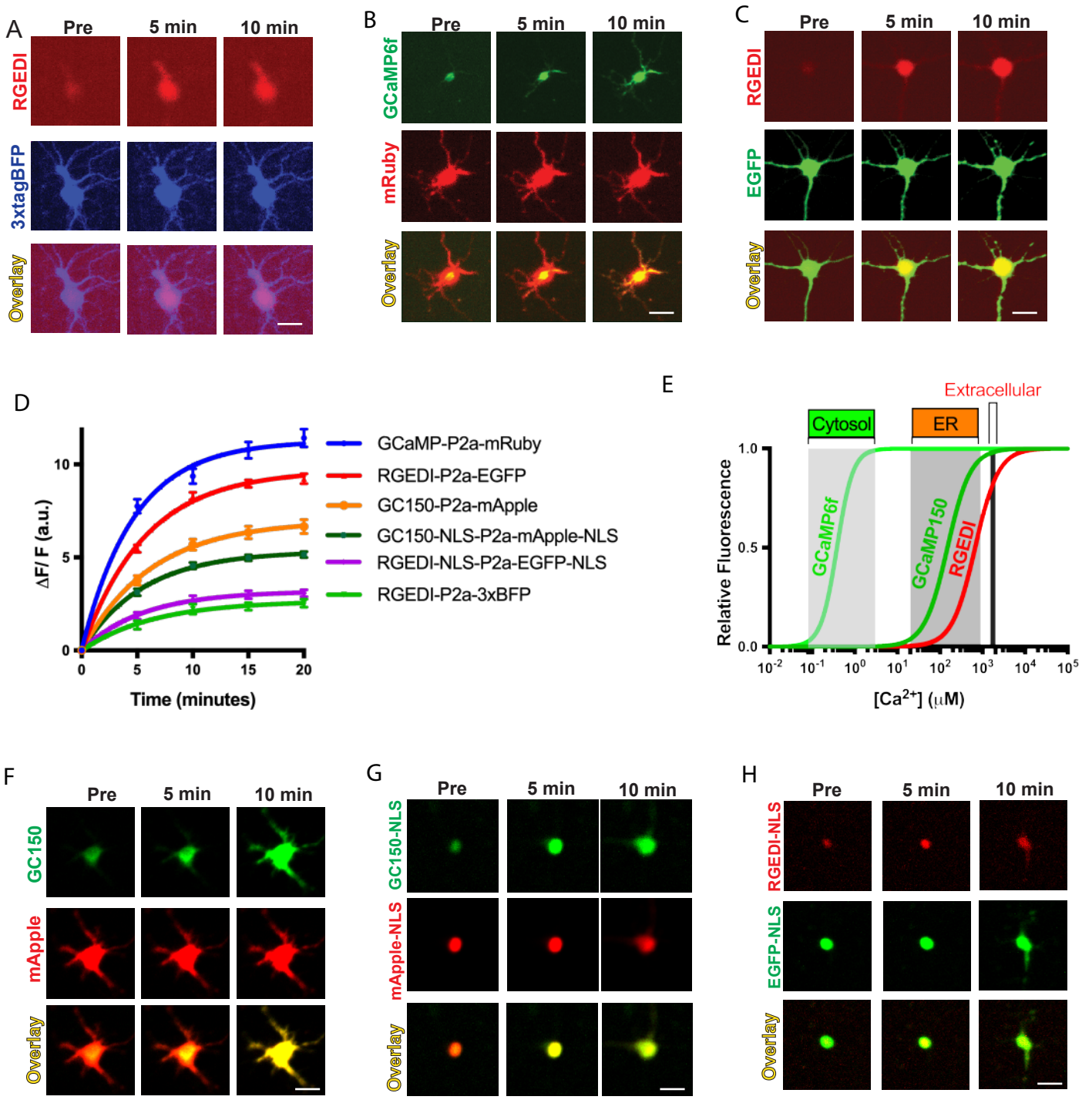
A
Pre
5 min
10 min
RGEDI
3xtagBFP
Overlay
B
Pre
5 min
10 min
GCaMP6f
mRuby
Overlay
C
Pre
5 min
10 min
RGEDI
EGFP
Overlay
D
ΔF/ F (a.u.)
Time (minutes)
GCaMP-P2a-mRuby
RGEDI-P2a-EGFP
GC150-P2a-mApple
GC150-NLS-P2a-mApple-NLS
RGEDI-NLS-P2a-EGFP-NLS
RGEDI-P2a-3xBFP
E
Extracellular
Cytosol
ER
Relative Fluorescence
GCaMP6f
GCaMP150
RGEDI
[Ca2+] (μM)
F
Pre
5 min
10 min
GC150
mApple
Overlay
G
Pre
5 min
10 min
GC150-NLS
mApple-NLS
Overlay
H
Pre
5 min
10 min
RGEDI-NLS
EGFP-NLS
Overlay

Figure 4

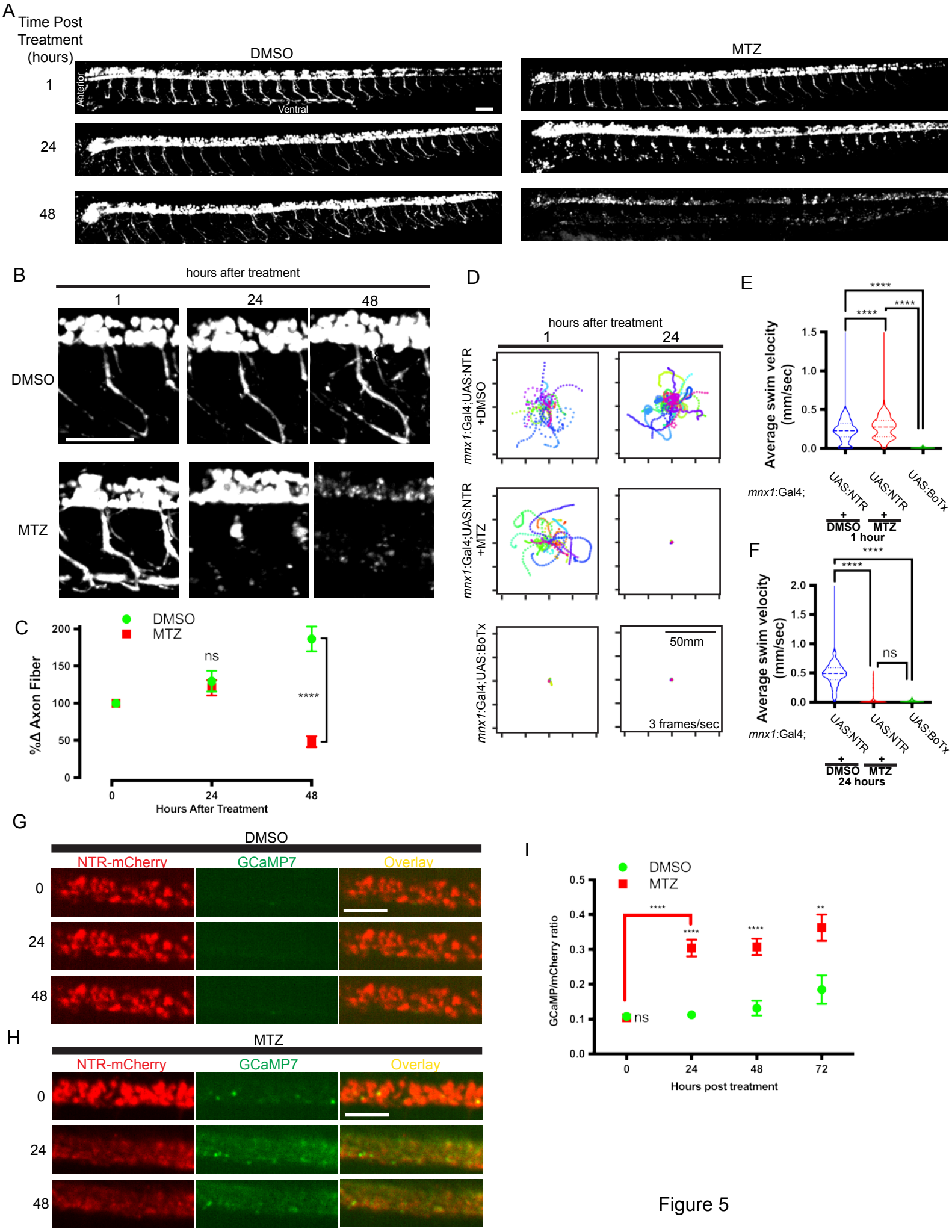
A
Time Post Treatment (hours)
DMSO
MTZ
1
24
48
Anterior
Ventral
B
hours after treatment
1
24
48
DMSO
MTZ
C
DMSO
MTZ
%Δ Axon Fiber
200
150
100
50
0
ns
****
0
24
48
Hours After Treatment
D
hours after treatment
1
24
mnx1:Gal4;UAS:NTR +DMSO
mnx1:Gal4;UAS:NTR +MTZ
mnx1:Gal4;UAS:BoTx
50mm
3 frames/sec
E
Average swim velocity (mm/sec)
1.5
1.0
0.5
0.0
****
****
****
mnx1:Gal4;
UAS:NTR
UAS:NTR
UAS:BoTx
+
DMSO
+
MTZ
1 hour
F
Average swim velocity (mm/sec)
2.0
1.5
1.0
0.5
0.0
****
****
ns
mnx1:Gal4;
UAS:NTR
UAS:NTR
UAS:BoTx
+
DMSO
+
MTZ
24 hours
G
DMSO
NTR-mCherry
GCaMP7
Overlay
0
24
48
H
MTZ
NTR-mCherry
GCaMP7
Overlay
0
24
48
I
DMSO
MTZ
GCaMP/mCherry ratio
0.5
0.4
0.3
0.2
0.1
0.0
****
****
****
**
ns
0
24
48
72
Hours post treatment

Figure 5

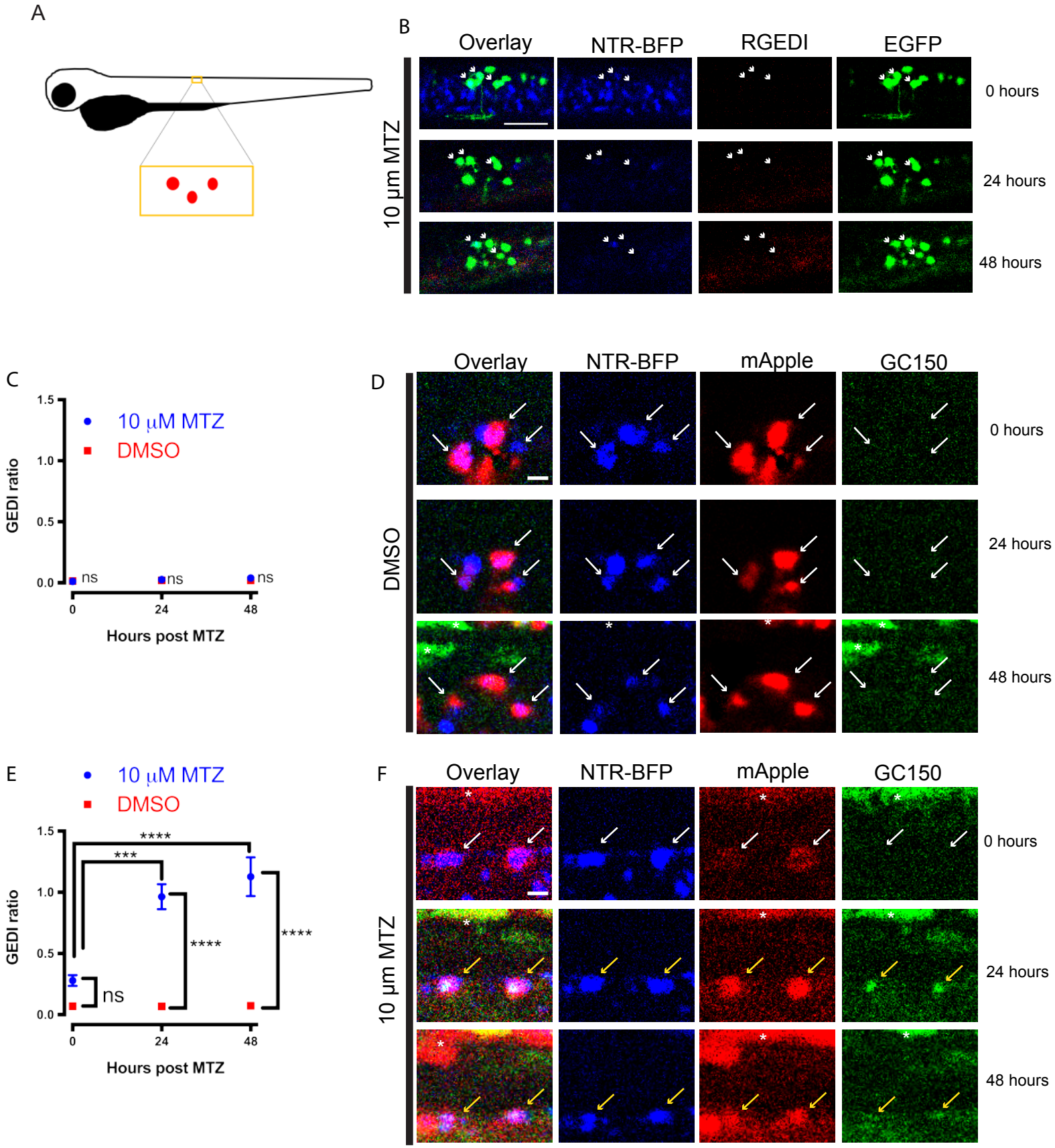
A
B
Overlay
NTR-BFP
RGEDI
EGFP
10 µm MTZ
0 hours
24 hours
48 hours
C
10 µM MTZ
DMSO
GEDI ratio
1.5
1.0
0.5
0.0
ns
ns
ns
0
24
48
Hours post MTZ
D
Overlay
NTR-BFP
mApple
GC150
DMSO
0 hours
24 hours
48 hours
E
10 µM MTZ
DMSO
GEDI ratio
1.5
1.0
0.5
0.0
****
***
****
****
ns
0
24
48
Hours post MTZ
F
Overlay
NTR-BFP
mApple
GC150
10 µm MTZ
0 hours
24 hours
48 hours

Figure 6